

# SPES: Spectrogram Perturbation for Explainable Speech-to-Text Generation

Dennis Fucci<sup>\*◇</sup>, Marco Gaido<sup>◇</sup>, Beatrice Savoldi<sup>◇</sup>,  
Matteo Negri<sup>◇</sup>, Mauro Cettolo<sup>◇</sup>, Luisa Bentivogli<sup>◇</sup>

<sup>\*</sup>University of Trento, Italy

<sup>◇</sup>Fondazione Bruno Kessler, Italy

{dfucci, mgaido, bsavoldi, negri, cettolo, bentivo}@fbk.eu

## Abstract

Spurred by the demand for interpretable models, research on eXplainable AI for language technologies has experienced significant growth, with feature attribution methods emerging as a cornerstone of this progress. While prior work in NLP explored such methods for *classification* tasks and *textual* applications, explainability intersecting *generation* and *speech* is lagging, with existing techniques failing to account for the autoregressive nature of state-of-the-art models and to provide fine-grained, phonetically meaningful explanations. We address this gap by introducing *Spectrogram Perturbation for Explainable Speech-to-text Generation (SPES)*, a feature attribution technique applicable to sequence generation tasks with autoregressive models. SPES provides explanations for each predicted token based on both the input spectrogram and the previously generated tokens. Extensive evaluation on speech recognition and translation demonstrates that SPES generates explanations that are faithful and plausible to humans.

## 1 Introduction

The recent advances of Artificial Intelligence (AI) and the emergence of foundation models (Bommasani et al., 2021) have come together with concerns about their risks and impact (Weidinger et al., 2021), as well as calls for a better understanding of their inner workings (Barredo Arrieta et al., 2020; Eiras et al., 2024). This need has been reinforced by the demands for transparency by legal frameworks like the EU AI Act and the US National AI Initiative Act (Panigutti et al., 2023; Roberts et al., 2024). In response, the field of eXplainable AI (XAI) has emerged prominently, with the goal of elucidating the reasoning behind system predictions (Doshi-Velez and Kim, 2017; Car-

valho et al., 2019; Vilone and Longo, 2021; Pradhan et al., 2022). Among the various active XAI approaches (Ferrando et al., 2024), this paper centers on *feature attribution* methods, which aim to identify and quantify the importance of each input feature in determining a model’s final output.

Originally developed for image and text classification (Danilevsky et al., 2020; Kamakshi and Krishnan, 2023), feature attribution methods have been extended to other modalities—like speech (Becker et al., 2024; Pastor et al., 2024)—and to text generation (Sarti et al., 2023; Zhao et al., 2024, et al.). Still, XAI in the domain of speech-to-text (S2T) generative tasks is limited, with only a few preliminary works focusing on automatic speech recognition (ASR) (Mandel, 2016; Trinh et al., 2018; Trinh and Mandel, 2021; Kavaki and Mandel, 2020; Markert et al., 2021; Wu et al., 2023, 2024). This contrasts with the pivotal role of spoken language—arguably the most natural form of human interaction (Munteanu et al., 2013)—and consequently with the importance of S2T technologies, which are now fostered by foundation models that transcribe and translate at an unprecedented scale (Latif et al., 2023).

Moreover, most existing feature attribution methods in S2T (Mandel, 2016; Trinh and Mandel, 2021; Markert et al., 2021; Wu et al., 2023, 2024) are not applied to autoregressive models, which predict each token iteratively, relying on both speech input and previous output tokens. Even the only method applied to autoregressive S2T models (Kavaki and Mandel, 2020) assumes conditional independence between prediction steps, disregarding the influence of previously generated text on each new prediction. Finally, these methods are either incompatible with the spectrogram input format (Markert et al., 2021; Wu et al., 2023, 2024), which is typically used in modern S2T models, or produce explanations that fail to highlight fine-grained patterns related to

acoustic characteristics of speech, such as the fundamental frequency and formants (Mandel, 2016; Trinh et al., 2018; Kavaki and Mandel, 2020; Trinh and Mandel, 2021).

To overcome the above limitations, we propose *Spectrogram Perturbation for Explainable Speech-to-text Generation* (SPES), the first feature attribution technique that provides token-level explanations for autoregressive S2T models by considering both the speech input and previously generated tokens.<sup>1</sup> SPES employs a perturbation-based approach that adapts image segmentation to spectrograms, enabling the identification of fine-grained, meaningful patterns. Through quantitative assessments and in-depth analyses across two S2T tasks—ASR and, for the first time, speech translation (ST)—we show that SPES produces accurate, phonetically interpretable explanations aligned with human understanding.

## 2 Background

Feature attribution methods produce a *saliency* score vector  $S = [s_1, s_2, \dots, s_d]$ , where each  $s_i$  represents the contribution of input feature  $x_i$  to the prediction  $y$  (Samek and Müller, 2019; Samek et al., 2021; Madsen et al., 2022).  $S$  is typically visualized as a heatmap, or *saliency map*, that highlights influential input regions. Existing methods fall into four categories: gradient-based, amortized, decomposition-based, and perturbation-based, each offering distinct ways to generate  $S$ .

*Gradient-based* methods (Simonyan et al., 2014; Sundararajan et al., 2017; Selvaraju et al., 2019) use the model’s gradients with respect to input features to measure feature importance, where the gradient reflects the sensitivity of the prediction to small changes in each feature. While these methods are efficient, as they involve a single or a few backpropagation steps, they can be unstable due to gradient instabilities and sensitivity to noise (Ancona et al., 2018; Samek et al., 2021; Dombrowski et al., 2022).

*Amortized explanation* methods (Dabkowski and Gal, 2017; Yoon et al., 2019; Schwarzenberg et al., 2021; Chuang et al., 2023b) train a global explainer to produce saliency maps in a single forward pass. Although efficient at inference time, this approach requires separate training for each model and depends on the explainer’s learning capacity, which can be influenced by biased training

patterns (Chuang et al., 2023a).

*Decomposition-based* methods (Bach et al., 2015; Shrikumar et al., 2017) propagate predictions backward through the network, layer by layer, decomposing the prediction score into contributions from individual neurons according to predefined rules. This process continues until the score is distributed across the input features. While these methods are as efficient as gradient-based ones, their effectiveness depends on the choice of propagation rules, which can vary across models and applications, potentially limiting their generalizability (Montavon et al., 2019).

*Perturbation-based* methods (Zeiler and Fergus, 2014; Lundberg and Lee, 2017; Fong and Vedaldi, 2017) determine feature saliency by systematically altering or masking parts of the input and observing the impact on the model’s output. Although computationally intensive, especially for high-dimensional data, they provide stable and accurate explanations independent of model architecture (Covert et al., 2021).

## 3 Related Works

Compared to other fields, feature attribution in S2T tasks has received relatively little attention, with efforts focused only on ASR, leaving other tasks like ST unexplored. Moreover, some of the proposed methods do not base their explanations on spectrograms, which is the standard input representation for state-of-the-art S2T models. Specifically, Markert et al. (2021) generate explanations based on mel-frequency cepstral coefficients, while Wu et al. (2023, 2024) generate them directly on raw waveforms.

Henceforth we focus on those feature attribution techniques that work with spectrograms. Spectrograms provide a 2D visualization of frequency distributions over time, where darker areas indicate higher energy at specific frequencies, capturing the acoustic characteristics of speech (Stevens, 2000). These techniques adopt either perturbation-based or amortized approaches.

The perturbation-based Bubble Noise technique introduced by Mandel (2016) and Trinh and Mandel (2021) obscures time-frequency patterns in the spectrogram using white noise, except in randomly positioned ellipsoidal bubble regions where the noise is attenuated, allowing speech characteristics to remain visible. To assess the impact of perturbations, this technique assigns a binary

<sup>1</sup>Code released under Apache 2.0 upon paper publication.

label to each predicted word based on whether the word changes under the perturbed input. Final saliency scores are calculated by correlating these labels with the noise mask, which tracks the amount of noise added to the spectrogram. Bubble Noise involves high computational costs to generate explanations, which escalate with increasing bubble counts. Additionally, the use of uniformly sized and shaped bubbles inherently overlooks the structural patterns within the spectrogram, potentially limiting the method’s effectiveness in capturing fine-grained acoustic details.

To reduce explanation time and provide fine-grained insights, [Trinh et al. \(2018\)](#) and [Kavaki and Mandel \(2020\)](#) propose an amortized explanation method based on perturbations. A mask estimator is trained to regulate white noise addition to individual features in the spectrogram aiming to maximize noise while preserving ASR accuracy. As a result, regions of the spectrogram where noise is minimized or absent are identified as salient for word prediction. However, in addition to the high costs associated with training separate explainers for different models, the resulting explanations highlight time-frequency patterns that only loosely correspond to acoustically meaningful characteristics ([Kavaki and Mandel, 2020](#)).

Besides the above limitations, both techniques lack adaptation to the autoregressive nature of modern S2T models, where each token generation depends on both input speech and prior output text. Leveraging the accuracy and architectural independence of perturbation-based methods, we fill these gaps by developing a technique that *i*) accounts for the autoregressive nature of modern S2T models, and *ii*) highlights fine-grained time-frequency patterns present in the spectrograms.

## 4 SPES

Given an autoregressive S2T model that generates one token at a time, conditioned on both the speech input  $X$ —represented as a spectrogram—and the previously generated tokens  $Y^{(k-1)} = [y_0, y_1, \dots, y_{k-1}]$ ,<sup>2</sup> SPES produces two saliency maps:  $S_{y_k}^X$ , which reveals the importance of input features across time and frequency, and  $S_{y_k}^{Y^{(k-1)}}$ , which highlights the importance of previously generated tokens. The overall explanation for the predicted sequence  $Y$ , comprising  $K$  tokens, is

<sup>2</sup>Where  $y_0$  is the special token start of sentence  $\langle s \rangle$ .

then formulated as:

$$S_Y = \{(S_{y_1}^X, S_{y_1}^{Y^0}), \dots, (S_{y_K}^X, S_{y_K}^{Y^{(K-1)}})\} \quad (1)$$

Preliminary experiments (detailed in Appendix A.2.2) indicated that separately perturbing the spectrogram and the previous output tokens yields more accurate saliency maps compared to joint perturbation. Therefore, we outline how these two components are perturbed independently to generate the corresponding saliency maps. Specifically, the following sections describe SPES in reference to the key components of perturbation-based approaches ([Covert et al., 2020](#)), namely *i*) selecting and perturbing features (§4.1), *ii*) estimating the impact of these perturbations on model predictions (§4.2), and *iii*) aggregating these impact estimations to derive final saliency scores (§4.3).

### 4.1 Input Perturbation

Input perturbation is usually performed by repeatedly masking input elements. However, perturbing each input element in combination with all others is impractical due to the exponential growth of possible combinations as the input size increases ([Khakzar et al., 2020](#); [Covert et al., 2021](#)). Therefore, perturbation-based approaches typically sample a subset of combinations, often employing techniques like Monte Carlo sampling ([Castro et al., 2017](#); [Petsiuk et al., 2018](#); [Markert et al., 2021](#); [Yang et al., 2021](#); [Fel et al., 2023](#)). Accordingly, we sample spectrogram features and previous output tokens for perturbation  $N^X$  and  $N^Y$  times, respectively, with  $N^X$  and  $N^Y$  serving as hyperparameters that balance the accuracy of the saliency map against computational costs.

#### 4.1.1 Perturbing Spectrograms

To achieve explanations that highlight fine-grained acoustic characteristics in spectrograms, we design perturbations that target time-frequency patterns using techniques from image processing, where morphological clustering is often employed to define the perturbation units ([Seo et al., 2020](#); [Yang et al., 2021](#)).<sup>3</sup> This approach produces explanations that align more naturally with object contours ([Ivanovs et al., 2021](#)), in contrast to perturbations with uniformly sized and shaped units. A

<sup>3</sup>In images, perturbations are typically applied either at the pixel level ([Wagner et al., 2019](#)) or to groups of pixels ([Zeiler and Fergus, 2014](#); [Ribeiro et al., 2016](#); [Yang et al., 2021](#)), referred to as *patches* or *superpixels*, which serve as the minimal processing units.

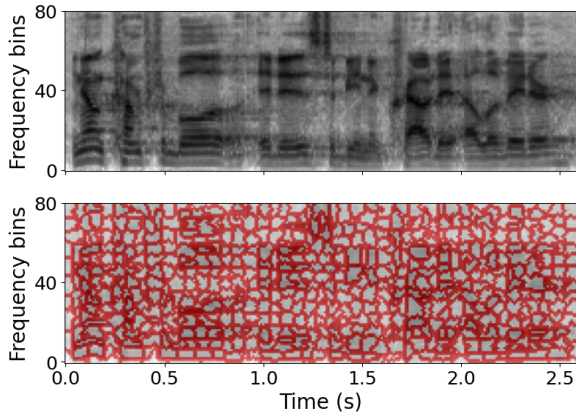


Figure 1: A mel-spectrogram (upper figure) and its segmentation obtained with SLIC (bottom figure).

particularly effective clustering-based technique is the *Morphological Fragmental Perturbation Pyramid* (MFPP; Yang et al. 2021), which generates detailed saliency maps (Ivanovs et al., 2021). MFPP employs Simple Linear Iterative Clustering (SLIC; Achanta et al. 2012), a  $k$ -means-based algorithm that groups pixels according to spatial and color characteristics—representing, in our case, proxies for spectral patterns. By iteratively adjusting the number of clusters ( $k$ ), the method produces a hierarchy of patches across varying granularities, from fine to coarse.

As shown in Fig. 1, our SLIC-based segmentation of the spectrogram clusters nearby features with similar energy levels into distinct patches that respect the structure of acoustic patterns, such as formants. Following MFPP, each spectrogram is segmented at three levels of granularity by varying  $k$ . This *multi-scale* approach creates patches at different resolutions, enabling the perturbation of neighboring features together or separately.

However, unlike images that have fixed dimensions, speech data vary in duration. Consequently, a fixed value of  $k$  would result in larger patches for longer audio samples, leading to coarser explanations. To address this, SPES scales  $k$  proportionally to input length, ensuring consistent patch sizes across varying speech sample lengths. However, this approach has a limitation: as the number of patch combinations grows exponentially with  $k$ , exhaustive exploration of the search space requires a corresponding increase in the number of perturbations  $N^X$ , which becomes computationally intractable for large values of  $k$ .<sup>4</sup> Insufficient

<sup>4</sup>As shown in Fig. 4 in Appendix B, the relationship be-

exploration, on the other hand, eventually lowers explanation quality (see Appendix A.2.3). To balance computational cost and effective exploration of patch combinations, SPES limits the increase of  $k$  by setting a maximum value. Specifically, with  $len(X)$  as the input length in seconds,  $\phi$  as the number of patches per second, and  $\tau$  as the threshold length in seconds,  $k$  is determined as:

$$k = \min(len(X), \tau) \cdot \phi \quad (2)$$

Once the patches are defined, we randomly perturb them in combination across  $N^X$  iterations. The number of patches perturbed at each iteration is controlled by a hyperparameter ( $p_{spec}$ ), which specifies the probability of perturbing each patch—for example, with  $p_{spec} = 0.5$ , approximately half of the patches are perturbed.

Perturbation is implemented by setting the elements of the patch to 0 in a binary mask  $M^X \in \{0, 1\}^{T \times C}$ , where  $T$  represents the time dimension and  $C$  represents the frequency dimension of  $X$ . The perturbed input  $X'$  is then obtained by element-wise multiplication of the original input  $X$  and  $M^X$ , which corresponds to setting the perturbed features to 0, the mean energy value in the utterance.<sup>5</sup> This perturbation method—the same used at training time by SpecAugment (Park et al., 2019), a common augmentation technique in most training settings, including ours—avoids introducing artifacts that fall outside the training distribution, helping the model remain robust to perturbations and aligning with strategies to prevent hallucinations during perturbations (Holzinger et al., 2022; Brocki and Chung, 2023).

#### 4.1.2 Perturbing Previous Output Tokens

Inspired by the effectiveness demonstrated in context mixing by the *value zeroing* (Mohebbi et al., 2023) perturbation strategy, which replaces selected token embeddings with zero vectors, SPES adopts the same approach for the perturbation of the previous output tokens. Specifically, for each of the  $N^Y$  iterations, it builds a binary mask

tween audio duration and computation time for generating explanations is quadratic, meaning that longer audio samples account for most of the computation time. Hence, increasing  $N^X$  with the audio length would substantially increase computational costs.

<sup>5</sup>In line with standard practices in current S2T systems (Communication et al., 2023, among others), all input spectrograms undergo cepstral mean-variance normalization (Vilkki and Laurila, 1998) before being fed into the model.

$M^{Y^{(k-1)}} \in \{0, 1\}^{(k-1) \times 1}$ , where each token is randomly selected for perturbation with probability  $p_{tok}$ , and the corresponding mask values are set to 0. The mask  $M^{Y^{(k-1)}}$  is then multiplied with the embedding matrix of the previous output tokens to obtain their perturbed version  $Y^{(k-1)'}$ .

## 4.2 Perturbation Impact Estimation

The importance of the features perturbed at each iteration is assessed by estimating how the perturbation impacts the model’s ability to predict the output. In classification tasks, two common methods are used for this estimation, both based on the probability assigned by the model to the target class. One method uses the target class probability as the saliency score for non-perturbed features (Zeiler and Fergus, 2014; Petsiuk et al., 2018; Yang et al., 2021), where a high score indicates that the perturbed features do not include information relevant to predicting the target class. Alternatively, the score is computed as the difference between the original probability (without perturbation) and the probability obtained with the perturbed input (Ancona et al., 2018; Seo et al., 2020). In this case, the score is assigned to the perturbed features, where a high score suggests that the model’s ability to recognize the target class is compromised in their absence.

In S2T tasks, assessing single-class probabilities corresponds to using the probability of the token being explained. We posit that this approach can be improved for two reasons. First, while classification tasks typically deal with a limited number of target classes, S2T tasks involve a BPE vocabulary (Sennrich et al., 2016) with thousands of tokens (Di Gangi et al., 2020; Fendji et al., 2022). This results in output probability distributions that are high-dimensional, dense vectors rather than sparse, peaked distributions (Zhao et al., 2023). Second, the decoding process of S2T models often employs beam search (Sutskever et al., 2014), where the tokens with the highest probability are not always selected, and perturbations can significantly affect the predicted sequence by altering the probabilities of initially-neglected tokens.

Therefore, drawing on mechanistic interpretability research (Conmy et al., 2023; Zhang and Nanda, 2024), SPES estimates perturbation impact ( $r^X$  for spectrograms and  $r^{Y^{(k-1)}}$  for previous output tokens) by computing the KL divergence (Kullback and Leibler, 1951) between the

probability distribution of an S2T model  $\Psi$  fed with the original inputs ( $X$  and  $Y^{(k-1)}$ ) and that obtained with their perturbed counterparts ( $X'$  and  $Y^{(k-1)'}$ ). Specifically:

$$\begin{aligned} r^X &= \text{KL} \left( \Psi(X, Y^{(k-1)}), \Psi(X', Y^{(k-1)}) \right) \\ r^{Y^{(k-1)}} &= \text{KL} \left( \Psi(X, Y^{(k-1)}), \Psi(X, Y^{(k-1)'}) \right) \end{aligned}$$

## 4.3 Scores Aggregation

Following MFPP, the  $r$  scores are aggregated across all perturbation iterations to produce the saliency maps:

$$S = \frac{\sum_{i=1}^N r_i (1 - M_i)}{\sum_{i=1}^N (1 - M_i)} \quad (3)$$

where  $S$  is either  $S^X$  or  $S^{Y^{(k-1)}}$  and, accordingly,  $M$  is either  $M^X$  or  $M^{Y^{(k-1)}}$ ,  $N$  is either  $N^X$  or  $N^Y$ , and  $r$  is either  $r^X$  or  $r^{Y^{(k-1)}}$ . Specifically, Eq. 3 sums the  $r$  scores assigned to the perturbed features ( $1 - M_i$ ) in the numerator and weights them by the number of times each feature is perturbed in the denominator.

Lastly, SPES applies two normalization steps. First, it applies z-score normalization to each token-level saliency map ( $S_{y_k}^X$  and  $S_{y_k}^{Y^{(k-1)}}$ ) independently. This step addresses the varying magnitudes of saliency scores across different tokens  $y_k$  in the same output  $Y$ , preventing disproportionate emphasis on specific tokens. This is especially beneficial when aggregating token-level explanations at the sentence level, such as through averaging, to create a single saliency map that reflects the importance of features for the entire predicted sentence. The effectiveness of this normalization has been validated on the validation set, as detailed in Appendix A.2.1. Second, SPES applies joint min-max normalization to  $S_{y_k}^X$  and  $S_{y_k}^{Y^{(k-1)}}$  for the same token  $y_k$ , scaling their scores to the  $[0, 1]$  range. This paired normalization ensures interaction between the two maps: if one map has higher scores for a token, the other map will correspondingly receive lower scores, thereby reflecting the relative importance of  $S_{y_k}^X$  and  $S_{y_k}^{Y^{(k-1)}}$  for predicting  $y_k$ .

## 5 Evaluating Explanations in S2T

Evaluating the quality of explanations is a complex task, ideally involving the assessment of several desirable properties across three dimensions: content, presentation, and user (Nauta et al.,

2023). Within the **content** dimension, the foremost property is *correctness*, also known as *faithfulness* (Tomsett et al., 2020) or *faithfulness* (Jacovi and Goldberg, 2020), which refers to “how well explanations match model reasoning” (Li et al., 2023). Moving to the **presentation** dimension, the quality of an explanation concerns not only its composition (“how something is explained”) but also its *compactness*, adhering to the “less is more” principle. Accordingly, explanations should highlight the smallest possible set of features and avoid the inclusion of redundant elements (Sun et al., 2020). Lastly, concerning the **user** dimension, a desirable property is *plausibility*, defined as “how convincing the explanation is to humans” (Jacovi and Goldberg, 2020).

In this work, we consider all three dimensions relevant to evaluating explanations. We inspect the content dimension by assessing faithfulness with the *deletion* metric, a popular method in classification tasks (Arras et al., 2017; Samek et al., 2017; Petsiuk et al., 2018; Tomsett et al., 2020; Samek et al., 2021; Gevaert et al., 2024) and also used in ASR (Trinh and Mandel, 2020). On the presentation axis, we measure compactness using the *size* metric. Finally, on the user axis, we assess plausibility through *dedicated analyses* discussed in §8.

**Deletion** This metric evaluates how quickly performance declines as input features, ranked by saliency scores, are gradually removed. This is shown through a curve, where a steeper drop indicates that the most important features were removed early. The area under the curve (AUC) reflects how well the explanation identifies key features—the lower the AUC, the better. Trinh and Mandel (2020) applied deletion to ASR explanations, adding noise to the most relevant features for each word in the output sentence. Thereby, they test whether the prediction of the target word changes under the noisy condition, while predictions for other words remain unaffected, since the noisy features are not expected to influence them. The process is repeated across various subsets of features with different saliency levels. However, this approach assumes conditional independence in predicting different words, an assumption that does not hold in state-of-the-art autoregressive S2T models, where early errors can impact subsequent predictions. To address this limitation, we adapt the deletion metric to remove features from the spectrogram based on their saliency at

the sentence level and evaluate performance on the entire sentence using standard ASR and ST metrics as measures of accuracy. Specifically, we incrementally zero out the most salient features at the sentence level from the spectrogram in steps of 5% and assess downstream performance across the entire test set. We use WER<sup>6</sup> for ASR and BLEU<sup>7</sup> (Papineni et al., 2002) for ST, and then measure the deletion AUC. Since WER decreases with better performance, while BLEU increases, faithful explanations should yield high AUC values for ASR and low AUC values for ST.

**Size** Size measures the compactness of an explanation as the percentage of input features identified as responsible for the model’s prediction. In classification tasks, this involves incrementally adding the features with the highest saliency scores until the model’s prediction matches the original (Sun et al., 2020). However, applying this approach in S2T tasks is complex since the output text changes continuously rather than in discrete steps as in classification. Wu et al. (2024) test two criteria to detect changes: *i*) WER greater than 0, which considers any modification—even irrelevant—as a prediction change, and *ii*) cosine similarity of SentenceBERT encodings lower than 0.5, which targets changes in output semantics. Since the choice of the similarity metric can lead to varying results and the optimal metric is debatable, we avoid isolating the subset of most salient features; instead, we assess explanation size across various subsets. To this aim, we calculate the percentage of features with saliency scores above a threshold ranging from 0 to 1 in 5% increments and compute the AUC of the resulting curve as a comprehensive score. Lower AUCs reflect more compact explanations, resulting in more concise and clear presentation (Nauta et al., 2023).

## 6 Experimental Setting

**Tasks and Data** We test SPES on S2T tasks with English audio, focusing on ASR and ST into German (en→de) and Spanish (en→es) to assess its effectiveness across varying monotonicity in word alignment.<sup>8</sup> For evaluation, we use the

<sup>6</sup>Computed with editdistance 0.6.1 (<https://github.com/roy-ht/editdistance>). Scores are capped at 100 to mitigate instability from excessively high scores due to long hallucinations.

<sup>7</sup>Computed with sacreBLEU 1.5.1 (Post, 2018).

<sup>8</sup>English and Spanish follow the SVO order, while German is an SOV language (Östling, 2015).

MuST-C corpus (Cattoni et al., 2021): the en→de v2 subset for ASR and en→de ST, and the en→es v1 subset for en→es ST due to the absence of v2.

**Models** The ASR and two ST systems share the same architecture, consisting of a Conformer encoder and a Transformer decoder, and are fed with 80-feature mel-spectrograms (see Appendix A.1 for details on hyperparameters, training configurations, and data). We opted not to use widely adopted foundation models like Whisper (Radford et al., 2023) or SeamlessM4T (Communication et al., 2023) for several reasons: *i*) comparability across tasks, as Whisper only supports English translations; *ii*) performance, as our models outperform SeamlessM4T on these tasks (see comparison in Appendix A.1); and *iii*) computational efficiency, since our smaller models are more suited for extensive experiments while keeping computational costs manageable.

**SPES Hyperparameters** SPES hyperparameters were estimated through validation (see Appendix A.2). Spectrograms were clustered into patches using SLIC with default parameters from the scikit-image implementation,<sup>9</sup> except for sigma ( $\sigma$ ), which was set to 0. We set  $\phi$  to 400, 500, and 600 for the three-level multi-scale clustering, while  $\tau$  was set to 7.5 for ASR and 5 for ST. The number of masking iterations,  $N^X$ , was set to 20,000 with  $p_{spec}$  at 0.5. For previous output tokens,  $N^Y$  was set to 2,000 with  $p_{tok}$  at 0.4.

**Baselines** We compare SPES against two baselines. First, a *feature-wise* method that randomly perturbs previous output tokens and spectrograms at the level of single features without morphological clustering, and estimates the perturbation impact with KL divergence. For a fair comparison, we set  $N^X$  to 20,000 and  $N^Y$  to 2,000, as in SPES, with  $p_{spec} = 0.7$  and  $p_{tok} = 0.1$ , optimized via validation (see Appendix A.3.1). Second, an enhanced version of the *Bubble Noise* technique that uses KL divergence as a perturbation impact estimator and is extended to also perturb the previous output tokens. Since Bubble Noise is significantly slower than SPES, especially at high bubble counts, we set  $N^X$  to 1,000. This value corresponds to that used by Trinh and Mandel (2020) and results in a runtime comparable to SPES with  $N^X$  set to 20,000. The number of bubbles per

second is set to 10, with each bubble measuring approximately 0.43 seconds in width and 31 mel bins in height, as validated in Appendix A.3.2.

## 7 Results

### 7.1 Overall Results

The upper rows of Table 1 present Deletion and Size AUC scores for the two implemented baselines (*feature-wise* and *Bubble Noise*) and compare them with SPES across ASR (en) and ST (en→de, en→es). Full deletion and size curves are provided in Fig. 5 and 6 in Appendix B.

Deletion and size scores reveal consistent trends across the three tasks. Looking at the baselines, we observe that the *feature-wise* method outperforms *Bubble Noise* in deletion scores, likely due to the differing number of perturbation iterations ( $N^X$ ) assigned to the two baselines (see §6). However, despite the significantly lower  $N^X$ , *Bubble Noise* surpasses *feature-wise* in size scores.

When comparing SPES to the baselines, it clearly excels. In terms of deletion scores, SPES outperforms the *feature-wise* baseline by 21.15 points in ASR and up to 6.58 points in ST (en→es). The improvements are even more pronounced relative to the *Bubble Noise* technique (27.52 points in ASR and 10.56 in ST en→es). SPES also demonstrates its superiority in the size metric, with differences of up to 19.25 and 14.61 in ST (en→de) compared to *feature-wise* and *Bubble Noise*, respectively. Since the comparison between SPES and *Bubble Noise* involves different  $N^X$  values, for the sake of fairness we carried out additional experiments using the same  $N^X$  value (1,000) for both SPES and *Bubble Noise*. The results, presented in Table 9 in Appendix B, confirm SPES’s superior performance under this condition as well. 🍀 Overall, **SPES demonstrates its capability to generate faithful and compact explanations**, accurately highlighting the input elements that are relevant to the S2T model’s predictions while avoiding the inclusion of redundant information.

### 7.2 Ablation Study

To better understand how each design choice impacts the faithfulness and compactness of SPES-generated explanations, we conduct an ablation study. Firstly, we vary the granularity of spectrogram perturbations by testing: *i*) single-level segmentation instead of multi-level (*– multi-scale*),

<sup>9</sup><https://scikit-image.org/docs/dev/api/skimage.segmentation.html>

	ASR (en)		ST (en→de)		ST (en→es)	
	Deletion (↑)	Size (↓)	Deletion (↓)	Size (↓)	Deletion (↓)	Size (↓)
feature-wise	71.39	47.85	8.79	48.53	9.03	46.00
Bubble Noise	65.02	36.92	10.85	43.89	13.01	43.04
SPES	<b>92.54</b>	<b>29.71</b>	<b>2.34</b>	<b>29.28</b>	<b>2.45</b>	<b>29.47</b>
– multi-scale	92.22	29.94	2.49	29.62	2.56	29.78
– clustering	90.73	33.31	2.84	33.09	2.93	32.90
– duration adaptation	92.37	30.45	2.35	31.10	2.46	30.95
– KL	87.44	29.85	4.76	30.98	4.99	30.74

Table 1: Deletion and Size scores for the *feature-wise* and the *Bubble Noise* baselines as well as for SPES and the solutions tested in the ablation study.

by using only 500 as  $\phi$ , *ii*) fixed grid segmentation<sup>10</sup> instead of clustering (*– clustering*), *iii*) removal of the duration-based patch adaptation of Eq. 2 (*– duration adaptation*), using a fixed number of patches (2,000, 2,500, and 3,000)<sup>11</sup> for all audio samples regardless of their duration. Lastly, we assess the contribution of KL divergence by replacing it with token-level probability difference—widely used in text applications (Sarti et al., 2023; Miglani et al., 2023)—as a method for estimating perturbation impact (*– KL*).

Table 1 (lower rows) presents the scores resulting from these variations. Looking at deletion, the largest performance drop across all tasks occurs when KL divergence is replaced with token-level probability difference (*– KL*). Ablating KL divergence reduces performance also in terms of size, although differences are less evident (ranging from 0.14 to 1.70 points). ✦ We can conclude that **using KL divergence to estimate perturbation impact is beneficial for producing explanations that are both more faithful and more compact**. Examining the ablations related to patch definition in the input spectrogram, we find that considering morphological aspects has the greatest impact. Indeed, fixed grid segmentation (*– clustering*) leads to decreased faithfulness for both ASR and ST, along with a 12-13% increase in explanation size across all tasks. ✦ This indicates that **accounting for morphology in spectrograms is crucial** for isolating patterns that models exploit for their predictions. ✦ **Adapting the number of patches to the input speech duration also proves beneficial**: with a fixed number of patches (*– duration adaptation*), deletion

scores are slightly worse but similar, and the size increases by 2-6%. ✦ Lastly, **using multiple segmentation levels improves both faithfulness and compactness**: ablating this option (*– multi-scale*) has a slight negative impact across all tasks, reflected in both deletion and size scores, with a degradation of approximately 1% in size for ST.

In summary, all the design choices of SPES contribute to providing faithful and compact explanations. Among them, estimating the impact of perturbations with KL divergence proves to be particularly crucial for achieving meaningful outcomes, followed by employing morphological clustering to define the units for perturbation.

## 8 Analyses of Plausibility

We assess the *plausibility* of SPES explanations by analyzing the saliency maps for both spectrograms ( $S^X$ ) and previously generated tokens ( $S^{Y^{(k-1)}}$ ). For  $S^X$ , we focus on ASR, where the more monotonic relationship between audio input and output tokens facilitates the analysis. For  $S^{Y^{(k-1)}}$ , we examine both ASR and ST.

### 8.1 Explanations for Spectrograms

**Time Dimension** Especially in ASR, manual inspection of  $S^X$  examples suggests that features’ saliency moves monotonically along the time dimension as the generation progresses from the first to the last token (for an example, see Appendix A.4). This observation aligns with the expectation that the generation is guided by the time frames in which the token is uttered, so explanations should be time-localized and shift from the start to the end of the audio sample. We verify this quantitatively by comparing word-level saliency maps on the

<sup>10</sup>Obtained setting the sigma parameter in SLIC, which determines the smoothness of the segmentation contours, to 10.

<sup>11</sup>Validated on the dev set, as described in Appendix A.2.1.

time axis<sup>12</sup> with word-level alignments provided by Gentle.<sup>13</sup> Specifically, we compare the mean score of the saliency maps for time frames *inside* and *outside* the boundaries indicated by Gentle, and test with a Student’s T-test the hypothesis that the mean score inside the time span is higher than that outside of the time span. ✦ As the test rejects the null hypothesis that the two means are equal with  $p < 0.01$ , we can assert that **SPES offers plausible insights on the time dimension.**

**Frequency Dimension** To assess whether SPES can also offer plausible insights along the frequency dimension, we analyze the distribution of explanation scores related to: *i*) phones exhibiting different spectral characteristics, and *ii*) same phones uttered by men and women.

In the first case, we select a *minimal pair* (Bale and Reiss, 2023) of words that differ in a single phoneme: *so* (/soʊ/) and *no* (/noʊ/).<sup>14</sup> The former features a voiceless alveolar sibilant /s/, characterized by turbulent airflow with high-frequency energy, typically above 4,000 Hz. The latter contains a voiced alveolar nasal /n/, exhibiting a low-frequency murmur, typically around 250-300 Hz (Keith, 2011). To check whether SPES highlights these specific characteristics, we select the explanations corresponding to the frames where these words are uttered, collect their maximum scores on the frequency axis, and average these values.<sup>15</sup> Results are plotted in Fig. 7 (top) in Appendix B. Several peaks over 0.5 points are noticeable. Some of them (e.g., around 500 and 1,200 Hz) are common to the two words, and reflect the typical frequency characteristics of back rounded vowels like those in the diphthong /oʊ/ (Hillenbrand et al., 1995). Others, instead, are peculiar of the two distinct phones: for *so*, scores are high above 4,000 Hz, as expected for alveolar sibilants, whereas *no* shows a prominent peak in the lower frequency region, around 300 Hz, corresponding to the murmur of an alveolar nasal (for examples of these

saliency maps, see Fig. 8 and 9 in Appendix B).

In Fig. 7 (bottom) in Appendix B, we compare saliency scores for men’s and women’s utterances of *so*. Due to the typically higher frequencies in women’s voices, linked to shorter vocal tract and smaller larynx size (Stevens, 2000), SPES’s saliency scores highlight slightly higher frequencies for women’s utterances compared to men’s.

✦ These analyses indicate that **SPES can offer valuable insights into the frequency dimension**, capturing phonetic differences between sounds and sociophonetic characteristics such as gender.

## 8.2 Spectrograms vs Previous Output Tokens

Previous analyses show that SPES-generated saliency maps generally localize salient areas effectively in both time and frequency domains. However, manual inspections revealed that some spectrogram saliency maps appear “noisy”, with scattered explanations that lack concentrated groups of features with higher saliency scores (for an example, see Appendix A.4). To investigate this behavior further, we explore whether this scattering is associated with specific token classes. Specifically, we hypothesize that, for some tokens, the less compact explanations in terms of speech features may stem from a higher contribution of previous output tokens to their prediction.

To quantify scattering, we use kurtosis, a measure of the “tailedness” of score distributions. Higher kurtosis indicates more peaked distributions, reflecting more focused explanations. For each token occurring over 100 times in the test set, we average the kurtosis values of all the spectrogram saliency maps related to its occurrences.

Interestingly, a trend emerges: tokens with higher kurtosis generally correspond to full words, while those with lower kurtosis are punctuation marks or special tokens. Fig. 10 shows the top and bottom 5 tokens by kurtosis. The bottom tokens include punctuation marks, the special end-of-sentence token `</s>`, and `_years`. The scattered explanations for these tokens suggests a lack of crucial audio information for their prediction. This is expected for punctuation, which often depends on grammatical rules rather than audio content. Similarly, `</s>` is always predicted based on a preceding strong punctuation mark, independent of the audio. In the case of `_years`, the model often relies on a preceding number in the output tokens, indicating a pattern-based prediction.

<sup>12</sup>To this aim, we first aggregate explanations at the word level by averaging the saliency maps of the tokens belonging to the same word, and then we take the maximum value over the frequency axis for each time frame.

<sup>13</sup><https://github.com/lowerquality/gentle>.

<sup>14</sup>We refer to the standard American English pronunciation, but we acknowledge that the actual pronunciation in individual samples may vary due to sociophonetic factors, including dialectal variations among speakers.

<sup>15</sup>The number of occurrences for *so* is 143, for *no* is 46.

📌 These findings reveal that **SPES can be used to determine whether a token is predicted based on the input speech or on the textual context**, as it highlights the dependency of a predicted token on previous ones only when plausible. In the next section, we further explore the plausibility of the textual relationships unveiled by SPES.

### 8.3 Explanations for Previous Output Tokens

**Positional Saliency** A manual inspection of  $S^{Y^{(k-1)}}$  in both ASR and ST revealed that two types of tokens typically receive higher saliency scores: the special start-of-sentence token  $\langle s \rangle$  and the latest token (LT), i.e., the token immediately preceding the one being explained (for an example, see Appendix A.4). Plotted distributions of the saliency scores for these token types and any tokens in intermediate positions (IT) reflect our qualitative insights: LTs have the highest mean (see Fig. 11 in Appendix B), followed by  $\langle s \rangle$ , whose distribution shifts towards higher scores compared to ITs. Student’s T-tests, comparing the means of these groups, always reject the null hypothesis of equal means with  $p < 0.01$ .

The importance of LTs underscores the critical role of the closest linguistic context. This finding is line with prior work that, by analyzing model component importance, demonstrated the significant focus of attention heads on LTs (Ferrando and Voita, 2024) and of final token states in terminal layers for predicting the subsequent tokens (Meng et al., 2022). Additionally, the significance of  $\langle s \rangle$  echoes findings from research on “attention sinks” in autoregressive language models, which suggest that initial tokens act as anchors due to their positional values (Xiao et al., 2024).

📌 In summary, concerning  $S^{Y^{(k-1)}}$ , **SPES highlights mechanisms that align with findings from previous research.**

**Intermediate Tokens** Despite the aforementioned trends in positional saliency, we observed instances where an IT holds the highest saliency score for the explanations of certain tokens (see Appendix A.4). To investigate this phenomenon, we analyze tokens occurring over 100 times in the test data for each task. For each unique token, we calculate the frequency with which an IT received the highest score in the explanation.

Table 10 presents examples from each language and task, showing the tokens where an IT held the highest score in at least 25% of their occurrences,

along with their top two most frequent ITs, if available. Overall, these explanations appear plausible and linguistically motivated. First, punctuation marks are present across all languages. The token  $\langle \cdot \rangle$  is explained by its complementary  $\langle \cdot \rangle$ . Similarly,  $\langle ? \rangle$  is explained by *What/what* in English, and by  $\langle \text{¿} \rangle$  in Spanish, i.e. by ITs that typically introduce questions. This signals that the preceding context plays a pivotal role in explaining token pairs that frequently co-occur. Also, it aligns with our findings on punctuation marks (§8.2): being characteristic of written text, punctuation does not have a direct correspondence in speech, reducing the saliency of the audio signal in the explanation.

By specifically looking at  $\text{en} \rightarrow \text{de}$ , the token  $\langle zu \rangle$  is preceded by the IT  $\langle \text{um} \rangle$  to create infinitive sentences. This German grammatical construction corresponds to the single token “to” in English (e.g., “*um Menschen aus ihren Stühlen zu holen*” – “to get people out of their chairs.”). Along the same line, the token  $\langle \text{an} \rangle$  acts as a separable prefix for the verb *fängt* (e.g. “*Es fängt später an*” – “it starts later”). Also,  $\langle \text{an} \rangle$  is part of fixed expressions like “*es fühlt sich so an*” (“it feels like”). 📌 These examples further demonstrate how **SPES relies on previous context to accurately interpret and explain tokens, particularly when there is no one-to-one mapping between source sentence and target translation.**

## 9 Conclusions

In response to the need for feature attribution methods specifically designed for S2T autoregressive models, this work introduces **SPES (Spectrogram Perturbation for Explainable Speech-to-text Generation)**. By employing a perturbation-based approach that ensures reliable explanations while remaining compatible with any model architecture, SPES produces token-level explanations throughout the predicted sentence. Its saliency maps are the first to effectively highlight contributions from fine-grained, acoustically meaningful patterns, such as formants, while also accounting for the influence of previous output tokens. We evaluate SPES on ASR and—for the first time—ST, and support this evaluation with in-depth analyses. Results show that SPES provides explanations that are faithful, compact, and plausible. This work contributes to enhancing the explainability of S2T models, laying groundwork for more transparent and reliable speech technology.

## References

- Radhakrishna Achanta, Appu Shaji, Kevin Smith, Aurelien Lucchi, Pascal Fua, and Sabine Süsstrunk. 2012. [SLIC Superpixels Compared to State-of-the-Art Superpixel Methods](#). *IEEE Transactions on Pattern Analysis and Machine Intelligence*, 34(11):2274–2282.
- Marco Ancona, Enea Ceolini, Cengiz Öztireli, and Markus Gross. 2018. [Towards better understanding of gradient-based attribution methods for Deep Neural Networks](#). In *Proceedings of the 6th International Conference on Learning Representations*, Vancouver, BC, Canada.
- Rosana Ardila, Megan Branson, Kelly Davis, Michael Kohler, Josh Meyer, Michael Henretty, Reuben Morais, Lindsay Saunders, Francis Tyers, and Gregor Weber. 2020. [Common Voice: A Massively-Multilingual Speech Corpus](#). In *Proceedings of the Twelfth Language Resources and Evaluation Conference*, pages 4218–4222, Marseille, France. European Language Resources Association.
- Leila Arras, Grégoire Montavon, Klaus-Robert Müller, and Wojciech Samek. 2017. [Explaining Recurrent Neural Network Predictions in Sentiment Analysis](#). In *Proceedings of the 8th Workshop on Computational Approaches to Subjectivity, Sentiment and Social Media Analysis*, pages 159–168, Copenhagen, Denmark. Association for Computational Linguistics.
- Sebastian Bach, Alexander Binder, Grégoire Montavon, Frederick Klauschen, Klaus-Robert Müller, and Wojciech Samek. 2015. [On Pixel-Wise Explanations for Non-Linear Classifier Decisions by Layer-Wise Relevance Propagation](#). *PLOS ONE*, 10(7):1–46.
- Alan Bale and Charles Reiss. 2023. *Phonology: A Formal Introduction*. The MIT Press.
- Alejandro Barredo Arrieta, Natalia Díaz-Rodríguez, Javier Del Ser, Adrien Bannetot, Siham Tabik, Alberto Barbado, Salvador Garcia, Sergio Gil-Lopez, Daniel Molina, Richard Benjamins, Raja Chatila, and Francisco Herrera. 2020. [Explainable Artificial Intelligence \(XAI\): Concepts, taxonomies, opportunities and challenges toward responsible AI](#). *Information Fusion*, 58:82–115.
- Sören Becker, Johanna Vielhaben, Marcel Ackermann, Klaus-Robert Müller, Sebastian Lapuschkin, and Wojciech Samek. 2024. [AudioMNIST: Exploring Explainable Artificial Intelligence for audio analysis on a simple benchmark](#). *Journal of the Franklin Institute*, 361(1):418–428.
- Rishi Bommasani, Drew A. Hudson, Ehsan Adeli, Russ Altman, Simran Arora, Sydney von Arx, Michael S. Bernstein, Jeannette Bohg, et al. 2021. [On the Opportunities and Risks of Foundation Models](#).
- Lennart Brocki and Neo Christopher Chung. 2023. [Feature perturbation augmentation for reliable evaluation of importance estimators in neural networks](#). *Pattern Recognition Letters*, 176:131–139.
- Diogo V. Carvalho, Eduardo M. Pereira, and Jaime S. Cardoso. 2019. [Machine Learning Interpretability: A Survey on Methods and Metrics](#). *Electronics*, 8(8).
- Javier Castro, Daniel Gómez, Elisenda Molina, and Juan Tejada. 2017. [Improving polynomial estimation of the shapley value by stratified random sampling with optimum allocation](#). *Computers & Operations Research*, 82:180–188.
- Roldano Cattoni, Mattia Antonino Di Gangi, Luisa Bentivogli, Matteo Negri, and Marco Turchi. 2021. [MuST-C: A multilingual corpus for end-to-end speech translation](#). *Computer Speech & Language*, 66:101155.
- Yu-Neng Chuang, Guanchu Wang, Fan Yang, Zirui Liu, Xuanting Cai, Mengnan Du, and Xia Hu. 2023a. [Efficient XAI Techniques: A Taxonomic Survey](#).
- Yu-Neng Chuang, Guanchu Wang, Fan Yang, Quan Zhou, Pushkar Tripathi, Xuanting Cai, and Xia Hu. 2023b. [CoRTX: Contrastive Framework for Real-time Explanation](#).
- Seamless Communication, Loïc Barrault, Yu-An Chung, Mariano Cora Meglioli, David Dale, et al. 2023. [SeamlessM4T: Massively Multilingual & Multimodal Machine Translation](#).
- Arthur Conmy, Augustine Mavor-Parker, Aengus Lynch, Stefan Heimersheim, and Adrià Garriga-Alonso. 2023. [Towards Automated](#)

- [Circuit Discovery for Mechanistic Interpretability](#). In *Advances in Neural Information Processing Systems*, volume 36, pages 16318–16352. Curran Associates, Inc.
- Ian C. Covert, Scott Lundberg, and Su-In Lee. 2020. Understanding global feature contributions with additive importance measures. In *Advances on Neural Information Processing Systems*, volume 33 of *NIPS '20*. Curran Associates, Inc.
- Ian C. Covert, Scott Lundberg, and Su-In Lee. 2021. Explaining by removing: a unified framework for model explanation. *The Journal of Machine Learning Research*, 22(1):9477–9566.
- Piotr Dabkowski and Yarín Gal. 2017. [Real Time Image Saliency for Black Box Classifiers](#). In *Advances in Neural Information Processing Systems*, volume 30. Curran Associates, Inc.
- Marina Danilevsky, Kun Qian, Ranit Aharonov, Yannis Katsis, Ban Kawas, and Prithviraj Sen. 2020. [A Survey of the State of Explainable AI for Natural Language Processing](#). In *Proceedings of the 1st Conference of the Asia-Pacific Chapter of the Association for Computational Linguistics and the 10th International Joint Conference on Natural Language Processing*, pages 447–459, Suzhou, China. Association for Computational Linguistics.
- Mattia A. Di Gangi, Marco Gaido, Matteo Negri, and Marco Turchi. 2020. [On Target Segmentation for Direct Speech Translation](#). In *Proceedings of the 14th Conference of the Association for Machine Translation in the Americas (Volume 1: Research Track)*, pages 137–150, Virtual. Association for Machine Translation in the Americas.
- Ann-Kathrin Dombrowski, Christopher J. Anders, Klaus-Robert Müller, and Pan Kessel. 2022. [Towards robust explanations for deep neural networks](#). *Pattern Recognition*, 121(C).
- Finale Doshi-Velez and Been Kim. 2017. [Towards A Rigorous Science of Interpretable Machine Learning](#).
- Francisco Eiras, Aleksandar Petrov, Bertie Vidgen, Christian Schroeder, Fabio Pizzati, Katherine Elkins, Supratik Mukhopadhyay, Adel Bibi, Aaron Purewal, Csaba Botos, Fabro Steibel, Fazel Keshtkar, Fazl Barez, Genevieve Smith, Gianluca Guadagni, Jon Chun, Jordi Cabot, Joseph Imperial, Juan Arturo Nolazco, Lori Landay, Matthew Jackson, Phillip H. S. Torr, Trevor Darrell, Yong Lee, and Jakob Foerster. 2024. [Risks and Opportunities of Open-Source Generative AI](#).
- Thomas Fel, Melanie Ducoffe, David Vigouroux, Rémi Cadène, Mikael Capelle, Claire Nicodème, and Thomas Serre. 2023. [Don't Lie to Me! Robust and Efficient Explainability with Verified Perturbation Analysis](#). In *2023 IEEE/CVF Conference on Computer Vision and Pattern Recognition (CVPR)*, pages 16153–16163.
- Jean Louis K. E Fendji, Diane C. M. Tala, Blaise O. Yenke, and Marcellin Atemkeng. 2022. [Automatic Speech Recognition Using Limited Vocabulary: A Survey](#). *Applied Artificial Intelligence*, 36(1):2095039.
- Javier Ferrando, Gabriele Sarti, Arianna Bisazza, and Marta R. Costa-jussà. 2024. [A Primer on the Inner Workings of Transformer-based Language Models](#).
- Javier Ferrando and Elena Voita. 2024. [Information Flow Routes: Automatically Interpreting Language Models at Scale](#).
- Ruth C. Fong and Andrea Vedaldi. 2017. [Interpretable Explanations of Black Boxes by Meaningful Perturbation](#). In *Proceedings of the IEEE International Conference on Computer Vision (ICCV)*, pages 3449–3457, Venice, Italy. IEEE Computer Society.
- Arne Gevaert, Axel-Jan Rousseau, Thijs Becker, Dirk Valkenburg, Tjil De Bie, and Yvan Saeys. 2024. [Evaluating feature attribution methods in the image domain](#). *Machine Learning*, 113(9):6019–6064.
- Alex Graves, Santiago Fernández, Faustino Gomez, and Jürgen Schmidhuber. 2006. [Connectionist temporal classification: labelling unsegmented sequence data with recurrent neural networks](#). In *Proceedings of the 23rd International Conference on Machine Learning*, page 369–376, Pittsburgh, Pennsylvania, USA. Association for Computing Machinery.

- Anmol Gulati, James Qin, Chung-Cheng Chiu, Niki Parmar, Yu Zhang, Jiahui Yu, Wei Han, Shibo Wang, Zhengdong Zhang, Yonghui Wu, and Ruoming Pang. 2020. [Conformer: Convolution-augmented Transformer for Speech Recognition](#). In *Proceedings of Interspeech 2020*, pages 5036–5040, Shanghai, China. International Speech Communication Association.
- François Hernandez, Vincent Nguyen, Sahar Ghannay, Natalia Tomashenko, and Yannick Estève. 2018. [TED-LIUM 3: Twice as Much Data and Corpus Repartition for Experiments on Speaker Adaptation](#). In *Speech and Computer*, pages 198–208, Leipzig, Germany. Springer International Publishing.
- James Hillenbrand, Laura Getty, Michael Clark, and Kimberlee Wheeler. 1995. [Acoustic characteristics of American English vowels](#). *The Journal of the Acoustical Society of America*, 97:3099–111.
- Andreas Holzinger, Anna Saranti, Christoph Molnar, Przemyslaw Biecek, and Wojciech Samek. 2022. [Explainable AI Methods - A Brief Overview](#). In *xxAI - Beyond Explainable AI: International Workshop, Held in Conjunction with ICML 2020*, pages 13–38, Vienna, Austria. Springer International Publishing.
- Javier Iranzo-Sánchez, Joan Albert Silvestre-Cerdà, Javier Jorge, Nahuel Roselló, Adrià Giménez, Albert Sanchis, Jorge Civera, and Alfonso Juan. 2020. [Europarl-ST: A Multilingual Corpus for Speech Translation of Parliamentary Debates](#). In *Proceedings of 2020 IEEE International Conference on Acoustics, Speech and Signal Processing (ICASSP)*, pages 8229–8233, Barcelona, Spain. The Institute of Electrical and Electronics Engineers, Inc.
- Maksims Ivanovs, Roberts Kadikis, and Kaspars Ozols. 2021. [Perturbation-based methods for explaining deep neural networks: A survey](#). *Pattern Recognition Letters*, 150:228–234.
- Alon Jacovi and Yoav Goldberg. 2020. [Towards Faithfully Interpretable NLP Systems: How Should We Define and Evaluate Faithfulness?](#) In *Proceedings of the 58th Annual Meeting of the Association for Computational Linguistics*, pages 4198–4205, Online. Association for Computational Linguistics.
- Vidhya Kamakshi and Narayanan C. Krishnan. 2023. [Explainable Image Classification: The Journey So Far and the Road Ahead](#). *AI*, 4(3):620–651.
- Hassan Salami Kavaki and Michael I. Mandel. 2020. [Identifying important time-frequency locations in continuous speech utterances](#). In *Interspeech 2020*, pages 1639–1643.
- Johnson Keith. 2011. *Acoustic and Auditory Phonetics*, 3rd edition edition. Wiley-Blackwell.
- Ashkan Khakzar, Soroosh Baselizadeh, Saurabh Khanduja, Christian Rupprecht, Seong Tae Kim, and Nassir Navab. 2020. [Improving Feature Attribution through Input-specific Network Pruning](#).
- Diederik P. Kingma and Jimmy Ba. 2015. Adam: A Method for Stochastic Optimization. In *Proceedings of the 3rd International Conference on Learning Representations*, San Diego, CA, USA.
- Taku Kudo and John Richardson. 2018. [SentencePiece: A simple and language independent subword tokenizer and detokenizer for Neural Text Processing](#). In *Proceedings of the 2018 Conference on Empirical Methods in Natural Language Processing: System Demonstrations*, pages 66–71, Brussels, Belgium. Association for Computational Linguistics.
- Solomon Kullback and Richard A. Leibler. 1951. [On Information and Sufficiency](#). *The Annals of Mathematical Statistics*, 22(1):79 – 86.
- Siddique Latif, Moazzam Shoukat, Fahad Shamshad, Muhammad Usama, Yi Ren, Heriberto Cuayáhuitl, Wenwu Wang, Xulong Zhang, Roberto Togneri, Erik Cambria, and Björn W. Schuller. 2023. [Sparks of Large Audio Models: A Survey and Outlook](#).
- Xuhong Li, Mengnan Du, Jiamin Chen, Yekun Chai, Himabindu Lakkaraju, and Haoyi Xiong. 2023. [M<sup>4</sup>: A Unified XAI Benchmark for Faithfulness Evaluation of Feature Attribution Methods across Metrics, Modalities and Models](#). In *Advances on Neural Information Processing Systems*, volume 36, pages 1630–1643,

- New Orleans, LA, USA. Curran Associates, Inc.
- Scott M. Lundberg and Su-In Lee. 2017. [A unified approach to interpreting model predictions](#). In *Advances on Neural Information Processing Systems*, volume 30, page 4768–4777, Long Beach, CA, USA. Curran Associates, Inc.
- Andreas Madsen, Siva Reddy, and Sarath Chandar. 2022. [Post-hoc Interpretability for Neural NLP: A Survey](#). *ACM Computing Surveys*, 55(8).
- Michael I. Mandel. 2013. [Learning an intelligibility map of individual utterances](#). In *2013 IEEE Workshop on Applications of Signal Processing to Audio and Acoustics*, pages 1–4.
- Michael I. Mandel. 2016. [Directly comparing the listening strategies of humans and machines](#). In *Interspeech 2016*, pages 660–664.
- Karla Markert, Romain Parracone, Mykhailo Kulakov, Philip Sperl, Ching-Yu Kao, and Konstantin Böttinger. 2021. [Visualizing Automatic Speech Recognition – Means for a Better Understanding?](#) In *Proceedings of the 2021 ISCA Symposium on Security and Privacy in Speech Communication*, pages 14–20, Virtual. International Speech Communication Association.
- Kevin Meng, David Bau, Alex Andonian, and Yonatan Belinkov. 2022. [Locating and editing factual associations in GPT](#). In *Advances on Neural Information Processing Systems*, volume 35, New Orleans, LA, USA. Curran Associates, Inc.
- Vivek Miglani, Aobo Yang, Aram Markosyan, Diego Garcia-Olano, and Narine Kokhlikyan. 2023. [Using Captum to Explain Generative Language Models](#). In *Proceedings of the 3rd Workshop for Natural Language Processing Open Source Software (NLP-OSS 2023)*, pages 165–173, Singapore. Association for Computational Linguistics.
- Hosein Mohebbi, Willem Zuidema, Grzegorz Chrupała, and Afra Alishahi. 2023. [Quantifying Context Mixing in Transformers](#). In *Proceedings of the 17th Conference of the European Chapter of the Association for Computational Linguistics*, pages 3378–3400, Dubrovnik, Croatia. Association for Computational Linguistics.
- Grégoire Montavon, Alexander Binder, Sebastian Lapuschkin, Wojciech Samek, and Klaus-Robert Müller. 2019. [Layer-wise relevance propagation: An overview](#). In Wojciech Samek, Grégoire Montavon, Andrea Vedaldi, Lars Kai Hansen, and Klaus-Robert Müller, editors, *Explainable AI: Interpreting, Explaining and Visualizing Deep Learning*, chapter 10, pages 193–209. Springer International Publishing, Cham.
- Cosmin Munteanu, Matt Jones, Sharon Oviatt, Stephen Brewster, Gerald Penn, Steve Whittaker, Nitendra Rajput, and Amit Nanavati. 2013. [We need to talk: HCI and the delicate topic of spoken language interaction](#). In *CHI '13 Extended Abstracts on Human Factors in Computing Systems*, page 2459–2464, Paris, France. Association for Computing Machinery.
- Meike Nauta, Jan Trienes, Shreyasi Pathak, Elisa Nguyen, Michelle Peters, Yasmin Schmitt, Jörg Schlötterer, Maurice van Keulen, and Christin Seifert. 2023. [From Anecdotal Evidence to Quantitative Evaluation Methods: A Systematic Review on Evaluating Explainable AI](#). *ACM Computing Surveys*, 55(13s).
- Robert Östling. 2015. [Word Order Typology through Multilingual Word Alignment](#). In *Proceedings of the 53rd Annual Meeting of the Association for Computational Linguistics and the 7th International Joint Conference on Natural Language Processing (Volume 2: Short Papers)*, pages 205–211, Beijing, China. Association for Computational Linguistics.
- Vassil Panayotov, Guoguo Chen, Daniel Povey, and Sanjeev Khudanpur. 2015. [Librispeech: An ASR corpus based on public domain audio books](#). In *Proceedings of 2015 IEEE International Conference on Acoustics, Speech and Signal Processing (ICASSP)*, pages 5206–5210, Brisbane, Queensland, Australia. The Institute of Electrical and Electronics Engineers, Inc.
- Cecilia Panigutti, Ronan Hamon, Isabelle Hupont, David Fernandez Llorca, Delia Fano Yela, Henrik Junklewitz, Salvatore Scalzo, Gabriele Mazzini, Ignacio Sanchez, Josep Soler Garrido, and Emilia Gomez. 2023. [The role of explainable AI in the context of the AI Act](#). In *Proceed-*

- ings of the 2023 ACM Conference on Fairness, Accountability, and Transparency, FAccT '23, page 1139–1150, New York, NY, USA. Association for Computing Machinery.
- Kishore Papineni, Salim Roukos, Todd Ward, and Wei-Jing Zhu. 2002. [BLEU: a Method for Automatic Evaluation of Machine Translation](#). In *Proceedings of the 40th Annual Meeting of the Association for Computational Linguistics*, pages 311–318, Philadelphia, Pennsylvania, USA. Association for Computational Linguistics.
- Daniel S. Park, William Chan, et al. 2019. [SpecAugment: A Simple Data Augmentation Method for Automatic Speech Recognition](#). In *Proceedings of Interspeech 2019*, Graz, Austria. International Speech Communication Association.
- Eliana Pastor, Alkis Koudounas, Giuseppe Atanasio, Dirk Hovy, and Elena Baralis. 2024. [Explaining Speech Classification Models via Word-Level Audio Segments and Paralinguistic Features](#). In *Proceedings of the 18th Conference of the European Chapter of the Association for Computational Linguistics (Volume 1: Long Papers)*, pages 2221–2238, St. Julian's, Malta. Association for Computational Linguistics.
- Vitali Petsiuk, Abir Das, and Kate Saenko. 2018. [RISE: Randomized Input Sampling for Explanation of Black-box Models](#). In *Proceedings of the British Machine Vision Conference (BMVC)*, Northumbria University, UK. The British Machine Vision Association and Society for Pattern Recognition.
- Matt Post. 2018. [A Call for Clarity in Reporting BLEU Scores](#). In *Proceedings of the Third Conference on Machine Translation: Research Papers*, pages 186–191, Brussels, Belgium. Association for Computational Linguistics.
- Romila Pradhan, Jiongli Zhu, Boris Glavic, and Babak Salimi. 2022. [Interpretable Data-Based Explanations for Fairness Debugging](#). In *Proceedings of the 2022 International Conference on Management of Data (SIGMOD)*, pages 247–261, Philadelphia, PA, USA. Association for Computing Machinery.
- Alec Radford, Jong Wook Kim, Tao Xu, Greg Brockman, Christine Mcleavey, and Ilya Sutskever. 2023. [Robust Speech Recognition via Large-Scale Weak Supervision](#). In *Proceedings of the 40th International Conference on Machine Learning*, volume 202, pages 28492–28518, Honolulu, Hawaii, USA. PMLR.
- Marco Tulio Ribeiro, Sameer Singh, and Carlos Guestrin. 2016. ["Why Should I Trust You?": Explaining the Predictions of Any Classifier](#). In *Proceedings of the 22nd ACM SIGKDD International Conference on Knowledge Discovery and Data Mining (KDD)*, page 1135–1144, San Francisco, California, USA. Association for Computing Machinery.
- Huw Roberts, Emmie Hine, Mariarosaria Taddeo, and Luciano Floridi. 2024. [Global AI governance: barriers and pathways forward](#). *International Affairs*, 100(3):1275–1286.
- Wojciech Samek, Alexander Binder, Grégoire Montavon, Sebastian Lapuschkin, and Klaus-Robert Müller. 2017. [Evaluating the Visualization of What a Deep Neural Network Has Learned](#). *IEEE Transactions on Neural Networks and Learning Systems*, 28(11):2660–2673.
- Wojciech Samek, Grégoire Montavon, Sebastian Lapuschkin, Christopher J. Anders, and Klaus-Robert Müller. 2021. [Explaining Deep Neural Networks and Beyond: A Review of Methods and Applications](#). *Proceedings of the IEEE*, 109(3):247–278.
- Wojciech Samek and Klaus-Robert Müller. 2019. [Towards Explainable Artificial Intelligence](#). In Wojciech Samek, Grégoire Montavon, Andrea Vedaldi, Lars Kai Hansen, and Klaus-Robert Müller, editors, *Explainable AI: Interpreting, Explaining and Visualizing Deep Learning*, chapter 1, pages 5–22. Springer International Publishing, Cham.
- Gabriele Sarti, Nils Feldhus, Ludwig Sickert, and Oskar van der Wal. 2023. [Inseq: An Interpretability Toolkit for Sequence Generation Models](#). In *Proceedings of the 61st Annual Meeting of the Association for Computational Linguistics (Volume 3: System Demonstrations)*, pages 421–435, Toronto, Canada. Association for Computational Linguistics.
- Robert Schwarzenberg, Nils Feldhus, and Sebastian Möller. 2021. [Efficient Explanations](#)

- from Empirical Explainers. In *Proceedings of the Fourth BlackboxNLP Workshop on Analyzing and Interpreting Neural Networks for NLP*, pages 240–249, Punta Cana, Dominican Republic. Association for Computational Linguistics.
- Ramprasaath R. Selvaraju, Michael Cogswell, Abhishek Das, Ramakrishna Vedantam, Devi Parikh, and Dhruv Batra. 2019. [Grad-CAM: Visual Explanations from Deep Networks via Gradient-Based Localization](#). In *Proceedings of the IEEE/CVF International Conference on Computer Vision (ICCV)*, pages 618–626, Seoul, South Korea. IEEE Computer Society.
- Rico Sennrich, Barry Haddow, and Alexandra Birch. 2016. [Neural Machine Translation of Rare Words with Subword Units](#). In *Proceedings of the 54th Annual Meeting of the Association for Computational Linguistics (Volume 1: Long Papers)*, pages 1715–1725, Berlin, Germany. Association for Computational Linguistics.
- Dasom Seo, Kanghan Oh, and Il-Seok Oh. 2020. [Regional Multi-Scale Approach for Visually Pleasing Explanations of Deep Neural Networks](#). *IEEE Access*, 8:8572–8582.
- Avanti Shrikumar, Peyton Greenside, and Anshul Kundaje. 2017. [Learning Important Features Through Propagating Activation Differences](#). In *Proceedings of the 34th International Conference on Machine Learning*, volume 70, pages 3145–3153, Sydney, NSW, Australia. PMLR.
- Karen Simonyan, Andrea Vedaldi, and Andrew Zisserman. 2014. Deep inside Convolutional Networks: Visualising Image Classification Models and Saliency Maps. In *Proceedings of the 2nd International Conference on Learning Representations*, Banff, AB, Canada.
- Kenneth N. Stevens. 2000. *Acoustic Phonetics*. The MIT Press.
- Youcheng Sun, Hana Chockler, Xiaowei Huang, and Daniel Kroening. 2020. [Explaining Image Classifiers Using Statistical Fault Localization](#). In *Computer Vision—ECCV 2020: 16th European Conference, Proceedings*, pages 391–406, Glasgow, UK. Springer International Publishing.
- Mukund Sundararajan, Ankur Taly, and Qiqi Yan. 2017. [Axiomatic attribution for deep networks](#). In *Proceedings of the 34th International Conference on Machine Learning*, pages 3319–3328, Sydney, NSW, Australia. PMLR.
- Ilya Sutskever, Oriol Vinyals, and Quoc V Le. 2014. [Sequence to Sequence Learning with Neural Networks](#). In *Advances on Neural Information Processing Systems*, volume 27, Montreal, QC, Canada. Curran Associates, Inc.
- Christian Szegedy, Vincent Vanhoucke, Sergey Ioffe, Jon Shlens, and Zbigniew Wojna. 2016. [Rethinking the Inception Architecture for Computer Vision](#). In *Proceedings of the 29th IEEE Conference on Computer Vision and Pattern Recognition (CVPR)*, pages 2818–2826, Las Vegas, NV, USA. IEEE Computer Society.
- Richard Tomsett, Dan Harborne, Supriyo Chakraborty, Prudhvi Gurram, and Alun Preece. 2020. [Sanity Checks for Saliency Metrics](#). *Proceedings of the AAAI Conference on Artificial Intelligence*, 34(04):6021–6029.
- Viet Anh Trinh and Michael Mandel. 2021. [Directly comparing the listening strategies of humans and machines](#). *IEEE/ACM Transactions on Audio, Speech, and Language Processing*, 29:312–323.
- Viet Anh Trinh and Michael I. Mandel. 2020. [Large scale evaluation of importance maps in automatic speech recognition](#). In *Interspeech 2020*, pages 1166–1170.
- Viet Anh Trinh, Brian McFee, and Michael I Mandel. 2018. [Bubble cooperative networks for identifying important speech cues](#). In *Interspeech 2018*, pages 1616–1620.
- Ashish Vaswani, Noam Shazeer, Niki Parmar, Jakob Uszkoreit, Llion Jones, Aidan N. Gomez, Łukasz Kaiser, and Illia Polosukhin. 2017. [Attention is All you Need](#). In *Advances in Neural Information Processing Systems*, volume 30. Curran Associates, Inc.
- Olli Viikki and Kari Laurila. 1998. [Cepstral domain segmental feature vector normalization for noise robust speech recognition](#). *Speech Communication*, 25(1):133–147.

- Giulia Vilone and Luca Longo. 2021. [Notions of explainability and evaluation approaches for explainable artificial intelligence](#). *Information Fusion*, 76:89–106.
- Jörg Wagner, Jan Mathias Köhler, Tobias Gindele, Leon Hetzel, Jakob Thaddäus Wiedemer, and Sven Behnke. 2019. [Interpretable and Fine-Grained Visual Explanations for Convolutional Neural Networks](#). In *Proceedings of the IEEE/CVF Conference on Computer Vision and Pattern Recognition (CVPR)*, pages 9089–9099, Long Beach, California, USA. IEEE Computer Society.
- Changhan Wang, Juan Pino, Anne Wu, and Jiatuo Gu. 2020a. [CoVoST: A Diverse Multilingual Speech-To-Text Translation Corpus](#). In *Proceedings of the Twelfth Language Resources and Evaluation Conference*, pages 4197–4203, Marseille, France. European Language Resources Association.
- Changhan Wang, Morgane Riviere, Ann Lee, Anne Wu, Chaitanya Talnikar, Daniel Haziza, Mary Williamson, Juan Pino, and Emmanuel Dupoux. 2021. [VoxPopuli: A Large-Scale Multilingual Speech Corpus for Representation Learning, Semi-Supervised Learning and Interpretation](#). In *Proceedings of the 59th Annual Meeting of the Association for Computational Linguistics and the 11th International Joint Conference on Natural Language Processing (Volume 1: Long Papers)*, pages 993–1003, Online. Association for Computational Linguistics.
- Changhan Wang, Yun Tang, Xutai Ma, Anne Wu, Dmytro Okhonko, and Juan Pino. 2020b. [Fairseq S2T: Fast Speech-to-Text Modeling with Fairseq](#). In *Proceedings of the 1st Conference of the Asia-Pacific Chapter of the Association for Computational Linguistics and the 10th International Joint Conference on Natural Language Processing: System Demonstrations*, pages 33–39, Suzhou, China. Association for Computational Linguistics.
- Laura Weidinger, John Mellor, Maribeth Rauh, Conor Griffin, Jonathan Uesato, Po-Sen Huang, Myra Cheng, Mia Glaese, Borja Balle, Atoosa Kasirzadeh, Zac Kenton, Sasha Brown, Will Hawkins, Tom Stepleton, Courtney Biles, Abeba Birhane, Julia Haas, Laura Rimell, Lisa Anne Hendricks, William Isaac, Sean Legassick, Geoffrey Irving, and Iason Gabriel. 2021. [Ethical and social risks of harm from Language Models](#).
- Xiaoliang Wu, Peter Bell, and Ajitha Rajan. 2023. [Explanations for Automatic Speech Recognition](#). In *Proceedings of 2023 IEEE International Conference on Acoustics, Speech and Signal Processing (ICASSP)*, Rhodes Island, Greece. The Institute of Electrical and Electronics Engineers, Inc.
- Xiaoliang Wu, Peter Bell, and Ajitha Rajan. 2024. [Can We Trust Explainable AI Methods on ASR? An Evaluation on Phoneme Recognition](#). In *ICASSP 2024 - 2024 IEEE International Conference on Acoustics, Speech and Signal Processing (ICASSP)*, pages 10296–10300.
- Guangxuan Xiao, Yuandong Tian, Beidi Chen, Song Han, and Mike Lewis. 2024. [Efficient Streaming Language Models with Attention Sinks](#).
- Qing Yang, Xia Zhu, Jong-Kae Fwu, Yun Ye, Ganmei You, and Yuan Zhu. 2021. [MFPP: Morphological Fragmental Perturbation Pyramid for Black-Box Model Explanations](#). In *Proceedings of the 25th International Conference on Pattern Recognition (ICPR)*, pages 1376–1383, Los Alamitos, CA, USA. IEEE Computer Society.
- Jinsung Yoon, James Jordon, and Mihaela van der Schaar. 2019. [INVASE: Instance-wise Variable Selection using Neural Networks](#). In *7th International Conference on Learning Representations, ICLR 2019, New Orleans, LA, USA, May 6-9, 2019*. OpenReview.net.
- Matthew D. Zeiler and Rob Fergus. 2014. [Visualizing and Understanding Convolutional Networks](#). In *Computer Vision – ECCV 2014 13th European Conference, Proceedings*, pages 818–833, Zurich, Switzerland. Springer International Publishing.
- Fred Zhang and Neel Nanda. 2024. [Towards Best Practices of Activation Patching in Language Models: Metrics and Methods](#).
- Haiyan Zhao, Hanjie Chen, Fan Yang, Ninghao Liu, Huiqi Deng, Hengyi Cai, Shuaiqiang

Wang, Dawei Yin, and Mengnan Du. 2024. [Explainability for Large Language Models: A Survey](#). *ACM Transactions on Intelligent Systems and Technology*, 15(2).

Shuai Zhao, Zhuoqian Liang, Jinming Wen, and Jie Chen. 2023. [Sparsing and Smoothing for the seq2seq Models](#). *IEEE Transactions on Artificial Intelligence*, 4(3):464–472.

## A Experimental Setting

### A.1 Model Implementation

In this section, we provide further details on the implementation of the ASR and ST models (see §6) used in our experiments.

**Models** Our models were implemented using the fairseq-S2T framework (Wang et al., 2020b). As audio features, we use log-compressed mel-filterbanks (80 channels), computed over windows of 25ms with a stride of 10ms using pykaldi.<sup>16</sup> We encode text into BPE (Sennrich et al., 2016) using SentencePiece (Kudo and Richardson, 2018) with a vocabulary size of 8,000 for English and 16,000 for Spanish and German. The length of audio features is reduced by a factor of 4 using two 1D convolutional layers with stride 2. The output of the convolutions is fed to a 12-layer Conformer (Gulati et al., 2020) encoder, and a 6-layer Transformer (Vaswani et al., 2017) decoder. We used 512 embedding features, 2,048 hidden features in the FFN, and a kernel size of 31 for Conformer convolutions. In total, the models have 113M parameters. As an objective, we minimize label-smoothed cross entropy (Szegedy et al., 2016) on the output of the decoder (using as a reference either the textual translation, for ST, or the transcripts, for ASR) with an auxiliary CTC (Graves et al., 2006) loss with the transcripts as reference, regardless of the target task, computed on the output of the 8th encoder layer. We optimize the model weights with the Adam optimizer (Kingma and Ba, 2015) ( $\beta_1 = 0.9$ ,  $\beta_2 = 0.98$ ) and Noam learning rate scheduler (Vaswani et al., 2017) (inverse square-root) starting from 0 and reaching the 0.002 peak in 25,000 warm-up steps. The input features are normalized with Utterance-level Cepstral Mean and Variance Normalization and, at training time, we apply SpecAugment (Park et al., 2019). We set dropout probability to 0.1. The ASR model was trained for 250,000 steps while the ST models, one for each language direction, were trained for 200,000 steps, as their encoder was initialized with that of the ASR model. All trainings were carried out on four NVIDIA A100 GPUs (40GB of RAM) with 40,000 tokens per mini-batch and 2 as update frequency. All models were obtained by averaging the last 7 checkpoints.

<sup>16</sup><https://github.com/pykaldi/pykaldi>.

**Data** Our ASR model is trained on the following datasets: CommonVoice (Ardila et al., 2020), LibriSpeech (Panayotov et al., 2015), TEDLIUM v3 (Hernandez et al., 2018), and VoxPopuli (Wang et al., 2021). For ST, instead, as training corpora we used MuST-C (Cattoni et al., 2021), EuroParl-ST (Iranzo-Sánchez et al., 2020), and CoVoST v2 (Wang et al., 2020a). Additionally, we translated the transcripts of the ASR datasets into the two target languages with the NeMo MT models.<sup>17</sup>

Table 2 reports the results of our models and compares them with SeamlessM4T (Communication et al., 2023).

	ASR WER (↓)	ST en→de BLEU (↑)	ST en→es BLEU (↑)
Ours	<b>10.8</b>	<b>30.7</b>	<b>34.9</b>
Seamless	15.8	23.0	31.8

Table 2: ASR (WER) and ST (BLEU) results of our models compared to SeamlessM4T on the MuST-C tst-COMMON set.

### A.2 Validation of SPES Hyperparameters

In this section, we describe the SPES hyperparameter validation process (see §6). Due to the high number and wide range of possible hyperparameter values, a full systematic evaluation was computationally prohibitive. Thus, we began with a manual inspection of explanations on a subset of MuST-C dev set samples, narrowing down value ranges for each hyperparameter and setting the perturbation iterations  $N^X$  and  $N^Y$  at 20,000 and 2,000, respectively, to balance explanation quality and computational cost.

Next, we conducted a systematic validation to select the best configuration using the *deletion* metric (see §5). We validated spectrogram perturbation hyperparameters, except for the threshold length  $\tau$ , in A.2.1 and output token perturbation hyperparameters in A.2.2. Given the reduced, yet still numerous, hyperparameter combinations after initial filtering, this validation used a subsample of 130 utterances, randomly chosen between 5 and 10 seconds to represent typical lengths and avoid rare length biases. Finally, we validated  $\tau$  on the full validation set for both ASR and ST tasks to

<sup>17</sup>[https://docs.nvidia.com/nemo-framework/user-guide/latest/nemotoolkit/nlp/machine\\_translation/machine\\_translation.html](https://docs.nvidia.com/nemo-framework/user-guide/latest/nemotoolkit/nlp/machine_translation/machine_translation.html).

examine behavior across diverse lengths.

### A.2.1 Perturbing Spectrograms

For the perturbation of spectrograms (see §4.1.1), we validate three parameters: *i*) the number of patches per second ( $\phi$ ), which determines the granularity of the perturbation; *ii*) the sigma value ( $\sigma$ ) in SLIC, which controls the smoothness of segmentation contours; *iii*) the perturbation probability ( $p_{spec}$ ), which defines the probability of each patch being perturbed at each iteration. At this stage, we also validated the effectiveness of applying standard normalization to the token-level saliency maps before aggregating them into a sentence-level explanation. Table 3 presents the deletion scores for all these aspects.

**Number of Patches per Second ( $\phi$ )** As described in §4, our segmentation of the spectrogram

$k$	$\sigma$	$P_{spec}$	Deletion ( $\uparrow$ )	
			w/o norm	w/ norm
500 1000 2000	0	0.3	91.75	91.90
		0.5	91.95	92.87
		0.7	84.90	91.94
	1	0.3	91.92	91.88
		0.5	92.29	93.32
		0.7	85.26	91.94
1000 1500 2000	0	0.3	93.38	93.09
		0.5	93.41	94.56
		0.7	84.49	92.45
	1	0.3	92.93	92.62
		0.5	93.71	94.71
		0.7	84.82	92.65
2000 2500 3000	0	0.3	93.73	93.28
		0.5	94.12	<b>95.37</b>
		0.7	83.02	91.88
	1	0.3	93.62	93.18
		0.5	93.78	95.05
		0.7	82.45	91.93
3000 3500 4000	0	0.3	92.99	92.51
		0.5	92.39	94.24
		0.7	80.01	90.25
	1	0.3	92.37	91.75
		0.5	91.35	93.94
		0.7	78.55	88.70
1000 2500 5000	0	0.3	92.56	92.07
		0.5	92.46	93.94
		0.7	83.00	91.06
	1	0.3	91.61	91.17
		0.5	92.29	93.87
		0.7	82.87	91.06
Avg.			89.47	<b>92.04</b>

Table 3: Deletion scores to validate  $k$ ,  $\sigma$ ,  $p_{spec}$ .

adopts a multi-scale approach, using three levels of granularity achieved using three  $\phi$  values. As our validation set is quite homogeneous in terms of duration (in the [5, 10] seconds range) and the validation procedure is computationally expensive, we do not adjust the number of patches based on duration and optimize three values for the numbers of clusters  $k$ . Then, we derive  $\phi$  by dividing the best  $k$  values by 5 seconds. This choice aims to maximize the performance of the approach with fixed number of patches in our ablation study (*- duration adaptation*, see §7.2), ensuring that our method is not advantaged by more favourable hyperparameters. Among the various configuration tested, the combination  $k = [2000, 2500, 3000]$  consistently yields better results with the only exception of the results obtained with  $p_{spec} = 0.7$ . Accordingly, our experiments with SPES use 400, 500, and 600 patches per second as the three clustering scales.

**Sigma ( $\sigma$ )** The preliminary manual inspection revealed that increasing  $\sigma$  above 1 results in patch shapes similar to grids. Therefore, we considered two values for  $\sigma$ : 0 and 1. The former, the default value in the SLIC implementation in scikit-image, provides sharper patch contours, while the latter smooths them. The best value for  $\sigma$  varies across the different configurations, with no clear trend emerging. This indicates that both values are effective in terms of perturbation. However, for the selected number of patches ( $k = [2000, 2500, 3000]$ ),  $\sigma = 0$  yields better results. For this reason, we set  $\sigma$  to 0 in our experiments.

**Perturbation Probability ( $p_{spec}$ )** The initial manual inspection revealed that high and low  $p_{spec}$  values do not produce good explanations. For this reason, we tested three  $p_{spec}$  values: 0.3, 0.5, and 0.7. In all configurations of the other hyperparameters, the intermediate value provided better results. This suggests that a  $p_{spec}$  of 0.3 may be too low, as the model remains robust with only a few perturbed features, while a value of 0.7 may result in excessive information loss. In light of this, a  $p_{spec}$  of 0.5 proves to be an effective compromise.

**Normalization** For each parameter combination, we computed the scores using token-wise standard normalization. As discussed in §4.2, normalization levels off the differences between the score distributions of different tokens, which depend on the original probability distributions. In most combinations (specifically 20 out of the 30

$p_{tok}$	Deletion ( $\uparrow$ )	
	Joint	Separate
0.1	83.72	94.49
0.2	79.77	94.48
0.3	77.48	94.45
<b>0.4</b>	74.36	<b>94.50</b>
0.5	71.02	94.49
0.6	69.79	94.48
0.7	66.57	94.47
0.8	63.31	94.42
0.9	62.71	94.42
Avg.	72.08	<b>94.47</b>

Table 4: Deletion scores to validate  $p_{tok}$  in SPES.

considered), including that with the highest score ( $k = [2000, 2500, 3000]$ ,  $\sigma = 0$ ,  $p_{spec} = 0.5$ ), normalization turns out to be beneficial, and, on average, the scores with normalization were 2.57 points higher than those without normalization. Therefore, when aggregating token-level explanations at the sentence level, we use token-level normalization by default.

In summary, the selected parameters for spectrogram perturbation are:  $\phi = [400, 500, 600]$ ,  $\sigma = 0$ , and  $p_{spec} = 0.5$ . Our validation also proved that normalizing the token-level saliency maps leads to better sentence-level explanations.

### A.2.2 Perturbing Previous Output Tokens

After determining an effective combination of parameters for the spectrogram perturbation, we moved to validate the perturbation of the previous output tokens (see §4.1.2). Specifically, we analyzed two aspects: *i*) whether it is better to jointly perturb the speech input and previous output tokens or not, and *ii*) determining the optimal value of the perturbation probability  $p_{tok}$ .

**Joint vs Separate Perturbation** Previous output tokens can be perturbed in two ways: jointly with the spectrogram or separately. In the joint approach, both the spectrogram features and the previous output tokens are perturbed simultaneously, potentially revealing interdependencies between them for next-token predictions, and saliency scores are accordingly assigned to the perturbed elements of both sides. However, since the previous tokens are fewer than the speech features, they are perturbed more frequently, which can “blur” explanations on the spectrogram. Table 4 presents the deletion scores for both joint and separate perturbations. The results consistently show higher

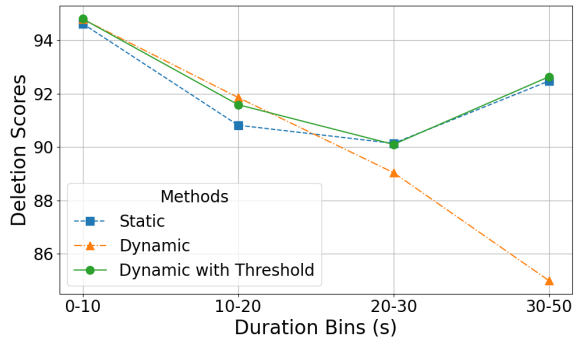


Figure 2: Variation of Deletion scores across samples of different lengths.

scores for separate perturbations, indicating that joint perturbation degrades performance. Consequently, in our experiments, we compute saliency scores separately for the speech input and the previous output tokens in SPES.

**Perturbation Probability ( $p_{tok}$ )** We considered  $p_{tok}$  values in the range  $[0.1, 0.9]$ . The differences in scores were slight (see Table 4). However, similar to the trend observed for  $p_{spec}$ , performance degradation was noted with values greater than 0.7, indicating that excessive information removal hinders effective perturbations. Unlike  $p_{spec}$ , lower values for  $p_{tok}$  were effective, most likely due to the lower cardinality and lower redundancy of information of the previous tokens compared to the features in the spectrograms. The best score was achieved with  $p_{tok}$  set to 0.4.

In summary, in all our experiments the previous output tokens are perturbed separately from the spectrogram, with  $p_{tok}$  equal to 0.4.

### A.2.3 Validation of the Dynamic Increase of Number of Patches and $\tau$

As discussed in §4.1.1, dynamically increasing the number of patches for long audio samples significantly raises the number of patch combinations, potentially reducing explanation quality. Fig. 2 shows deletion scores in ASR across input durations on the validation set, comparing a dynamic patch increase based on duration (*Dynamic*) versus a fixed number of patches (*Static*) with  $k$  set to  $[2,000, 2,500, 3,000]$ . While *Dynamic* performs better for samples up to 20 seconds, its deletion score declines linearly with duration. In contrast, *Static* remains stable scoring 7.49 points higher than *Dynamic* for samples over 30 seconds.

To mitigate this issue, we introduced the thresh-

$\tau$	Deletion		
	en ( $\uparrow$ )	en $\rightarrow$ de ( $\downarrow$ )	en $\rightarrow$ es ( $\downarrow$ )
2.5	93.01	2.47	2.91
<b>5.0</b>	93.91	<b>2.34</b>	<b>2.58</b>
<b>7.5</b>	<b>94.03</b>	2.41	2.62
10.0	93.91	2.49	2.77

Table 5: Deletion scores to validate the duration threshold  $\tau$  (in seconds) for stopping the linear increase in the number of patches.

$p_{spec}$	Deletion ( $\uparrow$ )
0.5	74.79
0.6	76.63
<b>0.7</b>	<b>79.29</b>
0.8	78.49
0.9	58.67

Table 6: Deletion scores to validate  $p_{spec}$  in the *feature-wise* configuration.

$p_{tok}$	Deletion ( $\uparrow$ )
<b>0.1</b>	<b>77.38</b>
0.2	77.31
0.3	77.29
0.4	77.21
0.5	77.17
0.6	77.18
0.7	77.21
0.8	77.10
0.9	77.06

Table 7: Deletion scores to validate  $p_{tok}$  in the *feature-wise* configuration.

old hyperparameter  $\tau$  (see §4.1.1), which limits dynamic increases in the number of patches beyond certain audio lengths. Table 5 presents the validation results for  $\tau$  on the full ASR and ST validation sets. For ASR, the optimal threshold is set at 7.5 seconds, while for ST, a lower threshold of 5.0 seconds is established. In Fig. 2, this *Dynamic with Threshold* approach effectively avoids the decline in faithfulness observed with *Dynamic*, consistently outperforming *Static* across all sample lengths, including those exceeding 30 seconds.

In summary, ASR uses  $k = [3, 000, 3, 750, 4, 500]$  for audio longer than 7.5 seconds, while ST uses  $k = [2, 000, 2, 500, 3, 000]$  for audio over 5.0 seconds.

### A.3 Validation of Baselines Hyperparameters

To ensure a fair comparison with SPES, we conducted a validation procedure to determine the optimal hyperparameters for the *feature-wise* and *Bubble Noise* baselines discussed in §6.

#### A.3.1 Feature-wise Perturbation

Since no segmentation of the spectrogram is involved in *feature-wise*, the only parameters to be validated are  $p_{spec}$  and  $p_{tok}$ . The preliminary manual inspection revealed that low values for  $p_{spec}$  were not effective in providing high deletion scores. Since the perturbation involves only sparse single features rather than groups of contiguous features (i.e., the patches), it is reasonable that the model is robust in recovering information even when a large percentage of features is perturbed. Therefore, we focused on values from 0.5 onward, whose deletion scores are shown in Table 6. The best result was achieved with 0.7.

Table 7 shows the deletion scores for  $p_{tok}$ , with the perturbation of the previous output tokens carried out separately, as in SPES. Similar to  $p_{tok}$  in SPES, the differences among the scores are low, with lower values generally providing higher scores. However, in this case,  $p_{tok}$  set to 0.1 yielded the highest result.

In summary, for the experiments with the *feature-wise* baseline reported in §7, we set  $p_{spec}$  to 0.7 and  $p_{tok}$  to 0.1.

#### A.3.2 Bubble Noise Perturbation

We implement the Bubble Noise perturbation method (Mandel, 2013; Trinh and Mandel, 2020, 2021), enhancing it to also produce explanations for previous output tokens (see §6). To perturb the spectrogram, we generate random noise that matches the intensity range of the speech input.<sup>18</sup> This noise replaces the spectrogram everywhere except within randomly placed ellipsoidal bubbles, where it is attenuated and then added back to the spectrogram.

Regarding bubble size and count, previous works use various numbers of bubbles per second, ranging from 18 to 80, all with a fixed size of 0.35 seconds and a height of approximately 180 Hz. We explore different configurations within a range that encompasses the values tested in earlier studies. Specifically, we aim to cover about

<sup>18</sup>We also tested white noise at various levels of SNR relative to the input spectrogram. However, noise matching the intensity range of the input spectrogram performed better.

Bub/s	Width (s)	Height (mel)	Deletion ( $\uparrow$ )
<b>10</b>	$\sim 0.43$	$\sim 31$	<b>69.40</b>
35	$\sim 0.25$	$\sim 15$	59.07
115	$\sim 0.13$	$\sim 9$	56.97

Table 8: Deletion scores to validate bubble size and count.

half of the spectrogram with noise, aligning with SPES’s perturbation level ( $p_{spec} = 0.5$ ). Table 8 presents deletion scores for three levels of bubble granularity tested with  $N^X = 1,000$ . The configuration with 10 bubbles per second yielded the best results, achieving deletion scores that were 10.33 and 12.43 points higher than the configurations with 35 and 115 bubbles per second, respectively.

In summary, Bubble Noise perturbation was set to 10 bubbles per second, each covering  $\sim 0.43$  seconds in width and  $\sim 31$  mel bins in height.

#### A.4 Examples of Explanations

Fig. 3 shows  $S^X$  and  $S^{Y^{(k-1)}}$  for the transcription and the translation into German of the utterance “So what was the next step?”. These visualizations highlight the following points, also detailed in §8.

1. Comparing ASR and ST  $S^X$  maps reveals similar patterns; for example, the German tokens *war*, *nächste*, and *Schritt* align with the English counterparts *was*, *next*, and *step*, indicating a reliance on similar phonetic sequences.
2. In ASR  $S^X$ , salient areas move forward with each token, showing a monotonic progression in time (see §8.1). This effect is less pronounced in ST due to differences in word order, such as German *Was* and *also* (en. *what* and *so*) reversing the English order.
3. Most  $S^X$  maps are frequency-localized. For instance, *So* (ASR) shows high saliency in the high-frequency range typical of alveolar sibilants and mid-frequency ranges for vowel formants (see §8.1 and Fig. 8).
4. Some  $S^X$  maps lack clear salient areas, such as those for *?* in both ASR and ST (see §8.2).
5. In  $S^{Y^{(k-1)}}$ , the first and last tokens generally exhibit high saliency, with some intermediate tokens showing similar effects (see §8.3). For example, in ASR, *?* is influenced by *what*, and in ST, *der* (en. *the*) by *war* (en. *was*).

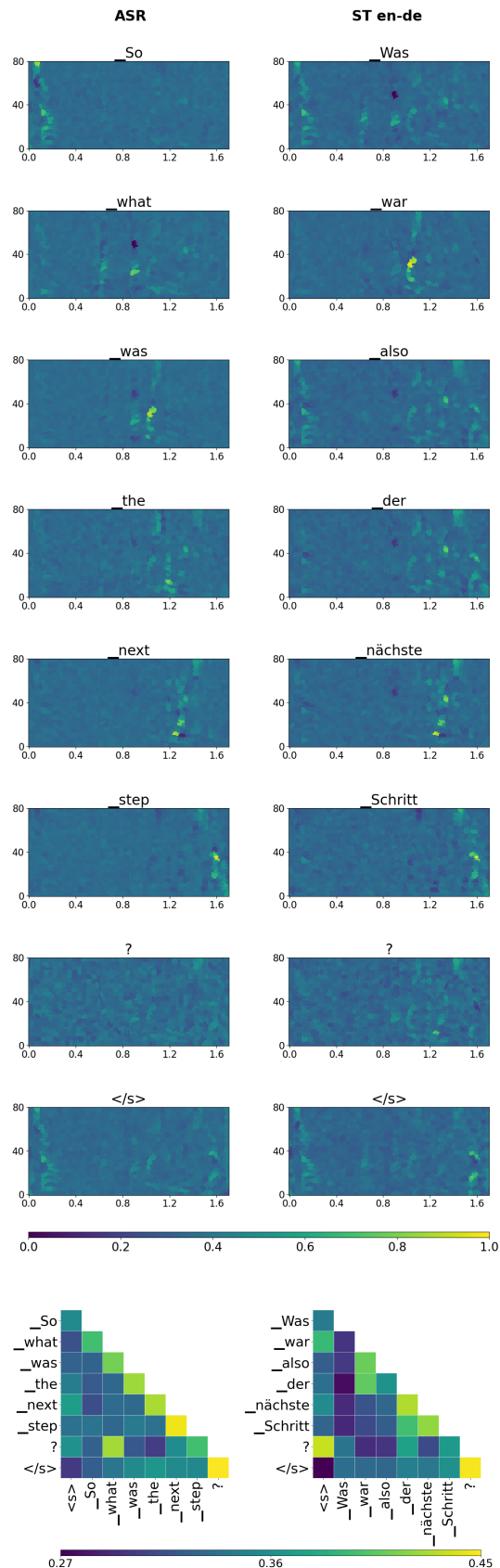


Figure 3:  $S^X$  (top) and  $S^{Y^{(k-1)}}$  (bottom) for ASR and ST on the utterance “So what was the next step?”. In  $S^{Y^{(k-1)}}$ , rows show the tokens being explained, and columns the previous output tokens.

## B Complementary Results

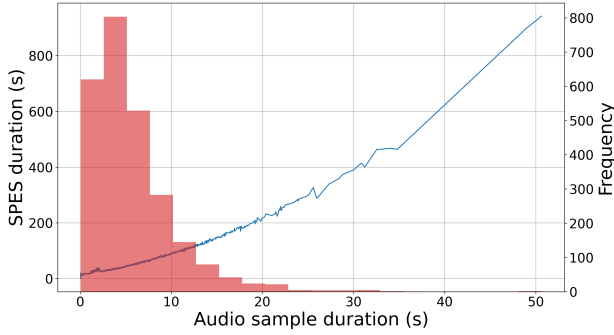
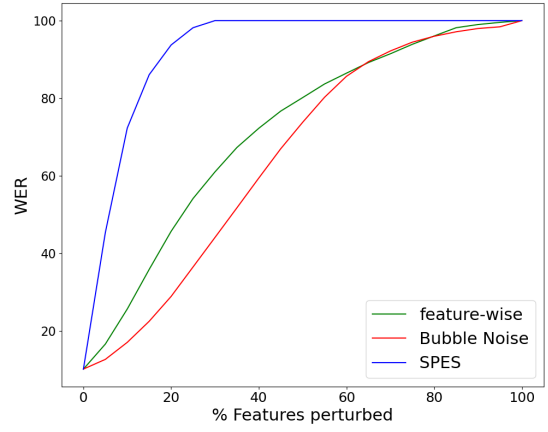


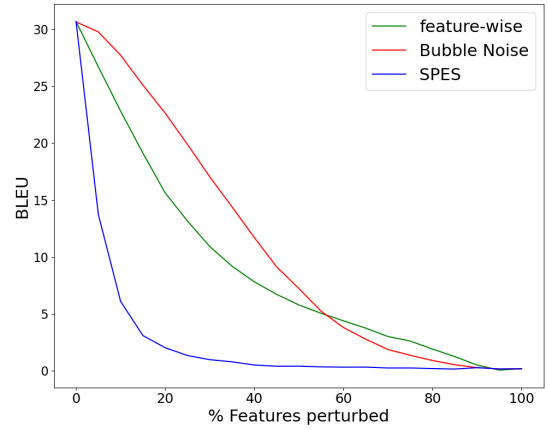
Figure 4: SPES explanation generation time across varying sample lengths and distribution of samples by length.

	ASR (en)	
	Deletion ( $\uparrow$ )	Size ( $\downarrow$ )
Bubble Noise	65.02	36.92
SPES fine-grained	75.22	39.54
SPES coarse-grained	<b>79.71</b>	<b>26.91</b>
	ST (en $\rightarrow$ de)	
	Deletion ( $\downarrow$ )	Size ( $\downarrow$ )
Bubble Noise	10.85	43.89
SPES fine-grained	6.84	40.06
SPES coarse-grained	<b>5.14</b>	<b>28.58</b>
	ST (en $\rightarrow$ es)	
	Deletion ( $\downarrow$ )	Size ( $\downarrow$ )
Bubble Noise	13.01	43.04
SPES fine-grained	7.41	39.66
SPES coarse-grained	<b>6.10</b>	<b>27.17</b>

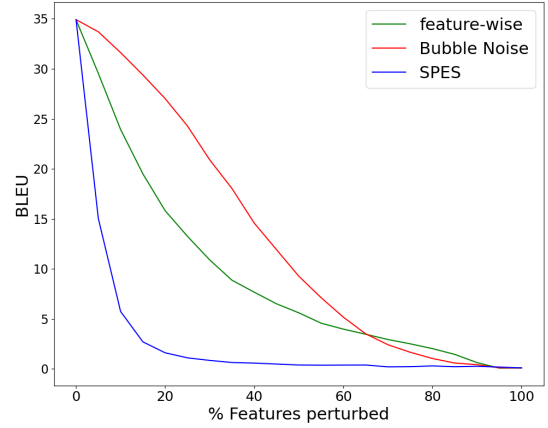
Table 9: Results comparing Bubble Noise and SPES with  $N^X = 1,000$ . SPES is evaluated in both a *fine-grained* setting ( $\phi$  validated in Appendix A.2.1) and a *coarse-grained* setting ( $\phi = [20, 40, 60]$ ), maintaining approximately 10 unperturbed patches per second—similar to Bubble Noise, which attenuates noise in 10 bubbles per second.



(a) ASR (en)

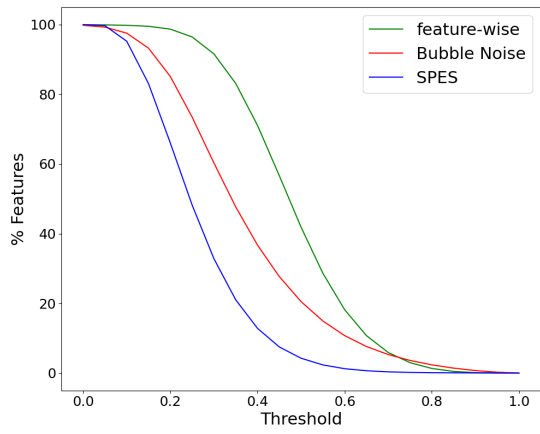


(b) ST (en $\rightarrow$ de)

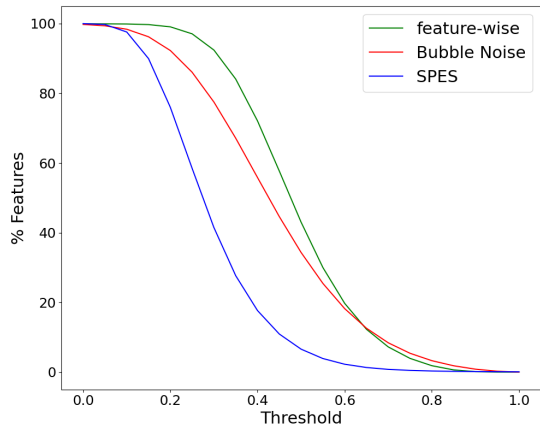


(c) ST (en $\rightarrow$ es)

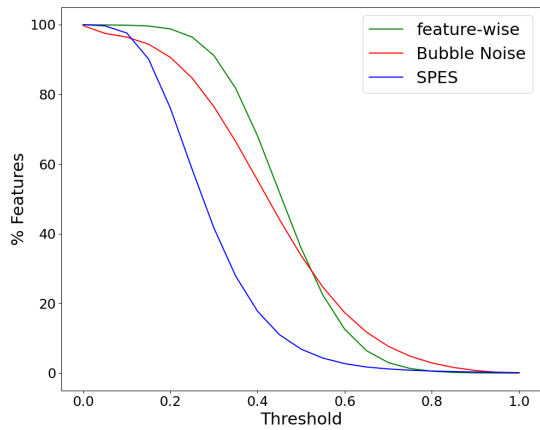
Figure 5: Deletion curves for the *feature-wise* strategy, the *Bubble Noise* technique, and SPES in the ASR and ST tasks.



(a) ASR (en)



(b) ST (en→de)



(c) ST (en→es)

Figure 6: Size curves for the *feature-wise* strategy, the *Bubble Noise* technique, and SPES in the ASR and ST tasks.

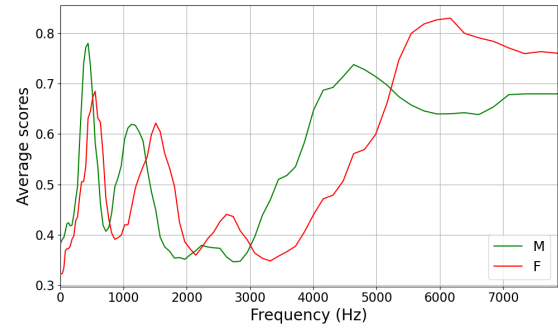
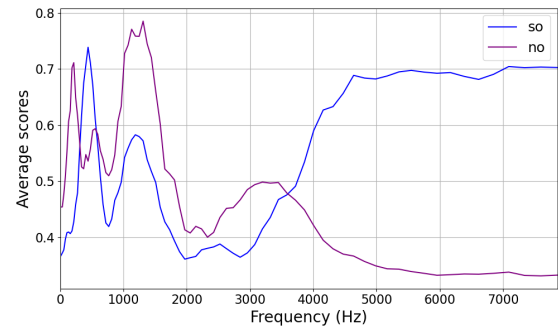


Figure 7: Average saliency scores over frequency for the minimal pair *so-no* (upper figure) and the word *so* uttered by men and women (lower figure).

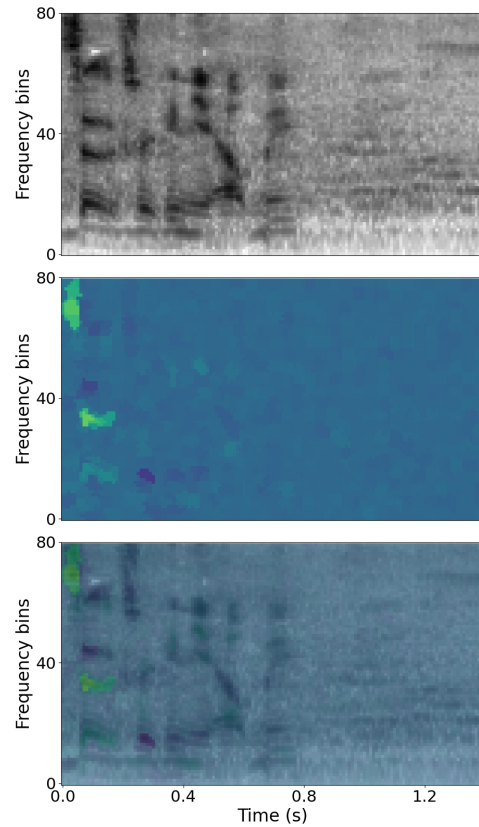


Figure 8: Example of saliency map (middle) for the token *so* (ASR), along with the corresponding spectrogram (top) and the map overlaid on the spectrogram (bottom).

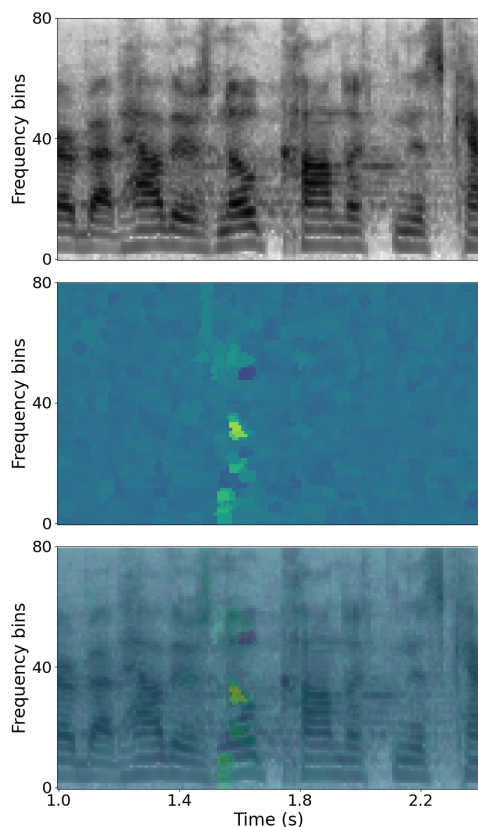


Figure 9: Example of saliency map (middle) for the token `no` (ASR), along with the corresponding spectrogram (top) and the map overlaid on the spectrogram (bottom).

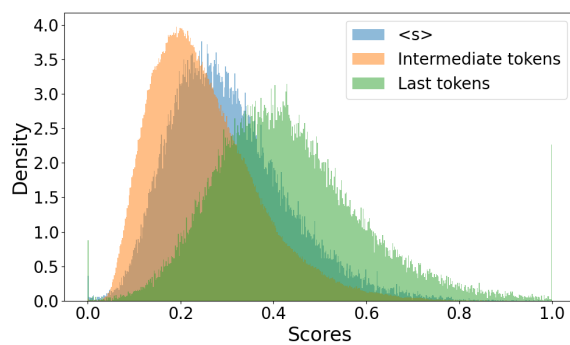


Figure 11: Distributions of saliency scores obtained in ST ( $en \rightarrow de$ ) for three types of tokens: `<s>`, *intermediate tokens* and tokens preceding the token to be explained (*last tokens*).

Task	Token	IT	%
ASR <i>en</i>	)	( [47]	40.5
	?	<b>What</b> [11], <b>what</b> [7]	29.1
ST $en \rightarrow es$	?	¿ [35], "¿ [7],	82.2
	)	( [148]	33.1
ST $en \rightarrow de$	)	( [105]	87.6
	<b>zu</b>	<b>um</b> [23], <b>zu</b> [11],	29.3
	<b>an</b>	<b>sich</b> [6], <b>fängt</b> [4]	25.1

Table 10: Tokens for which the highest saliency score is more often held by an IT. For each token, we provide the overall number of times it is primarily explained by *any* IT (%), and the frequency of each *individual* IT in holding the highest saliency in brackets.

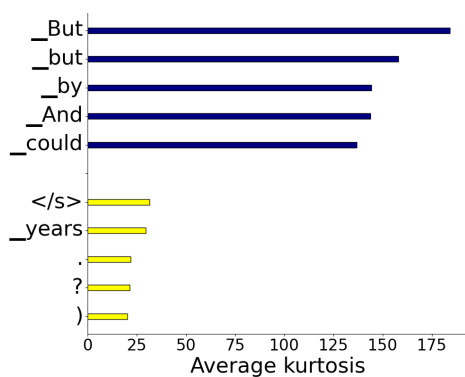


Figure 10: Top and bottom 5 tokens by kurtosis.